International Journal of Biological Macromolecules 363 (2026) 152190

Contents lists available at ScienceDirect

International Journal of Biological Macromolecules

journal homepage: www.elsevier.com/locate/ijbiomac

Advanced treatment for articular cartilage lesions: Development of an injectable glucosinolate-releasing hyaluronic acid

Laura Gambari [a,1], Cecilia Velino [b,1], Roberto Gotti [c], Luana Di Lisa [b], Lucia Ferrazzano [b], Dario Corbisiero [b], Alessandra Tolomelli [b], Alessandro Panciera [d], Cesare Faldini [d], Alberto Ruffilli [d], Martina D'Alessandro [a], Brunella Grigolo [a], Chiara Gualandi [b,e,*], Giovanna Desando [a,1,**], Maria Letizia Focarete [b,f,1]

[a] IRCCS Istituto Ortopedico Rizzoli, Laboratorio RAMSES, via di Barbiano 1/10, 40136, Bologna, Italy
[b] Department of Chemistry "G. Ciamician" and INSTM UdR of Bologna, University of Bologna, via Gobetti 85, 40129, Bologna, Italy
[c] Department of Pharmacy and Biotechnology FABIT, University of Bologna, via Belmeloro 6, 40126, Bologna, Italy
[d] IRCCS Istituto Ortopedico Rizzoli, 1st Orthopaedic and Traumatology Clinic, via G.C. Pupilli 1, 40136, Bologna, Italy
[e] Interdepartmental Center for Industrial Research on Advanced Applications in Mechanical Engineering and Materials Technology, CIRI-MAM, University of Bologna, Viale Risorgimento, 2, 40136, Bologna, Italy
[f] Health Sciences & Technologies (HST) CIRI, University of Bologna, Via Tolara di Sopra 41/E, 40064, Ozzano Emilia Bologna, Italy

ARTICLE INFO

Keywords:
Articular cartilage lesions
Microstructured hyaluronic acid hydrogel
Glucosinolates

ABSTRACT

Intra-articular injection of hyaluronic acid (HA) is commonly used to treat early-stage articular cartilage lesions (ACLs). While effective in restoring mechanical function, its long-term efficacy is limited by short stability and modest chondroprotective activity. A promising approach to enhance clinical outcomes is to combine HA with bioactive compounds. Here, we developed a novel microstructured HA (HA-MP_{HA}-BGL) that releases benzyl-glucosinolate (BGL), a glucosinolate (GLS) derived from the *Brassicaceae* family. HA-MP_{HA}-BGL was designed to fulfil two essential requirements for cartilage repair: (i) improving the physicochemical properties of HA to prolong its stability through the incorporation of HA crosslinked microparticles, and (ii) boosting its chondroprotective potential by exploiting the bioactivity of BGL. Additionally, HA-MP_{HA}-BGL was designed for targeting GLS directly to the articular site, thus overcoming the limitations associated with oral supplementation. HA-MP_{HA}-BGL demonstrated good rheological characteristics and exhibited resistance to enzymatic degradation in vitro. Biological assays demonstrated its cytocompatibility and chondroprotective effects on human joint cells: HA-MP_{HA}-BGL increased the expression of type 2 collagen, the major component of cartilage matrix, and reduced the expression of degenerative markers such as type 1 and 10 collagens, matrix metalloproteinase-13 (MMP-13), and A Disintegrin and Metalloproteinase with Thrombospondin motifs 5 (ADAMTS-5) in mesenchymal stromal cells. Furthermore, HA-MP_{HA}-BGL mitigated inflammation by reducing the nuclear factor kappa-light-chain-enhancer of activated B cells (NFkβ) pathway in a co-culture of chondrocytes and synoviocytes. As a prototype of GLS-releasing HA, HA-MP_{HA}-BGL represents a significant advancement in infiltrative therapies and lays the ground for further research on GLS-based treatments for ACLs.

1. Introduction

Articular cartilage lesions (ACLs) of the knee encompass a spectrum of damage, ranging from focal defects to advanced degenerative diseases, and are recognized as a relevant orthopaedic problem worldwide [1]. ACLs are mostly caused by trauma and osteoarthritis (OA) [2] and, to a lesser extent, by osteonecrosis and osteochondritis dissecans [1,2]. Because of its avascular nature, articular cartilage (AC) has

* Correspondence to: C. Gualandi, Department of Chemistry "G. Ciamician" and INSTM UdR of Bologna, University of Bologna, via Gobetti 85, 40129, Bologna, Italy.
** Correspondence to: G. Desando, IRCCS Istituto Ortopedico Rizzoli, Laboratorio RAMSES, via di Barbiano 1/6, 40136, Bologna, Italy.
E-mail addresses: c.gualandi@unibo.it (C. Gualandi), giovanna.desando@ior.it (G. Desando).
[1] These authors contributed equally to this work.

https://doi.org/10.1016/j.ijbiomac.2026.152190
Received 5 October 2025; Received in revised form 10 March 2026; Accepted 21 April 2026
Available online 23 April 2026

limited access to growth factors and cells necessary for healing, which leads to a poor capacity for self-repair during ACLs [3,4]. The most critical concern is ACLs' triggered joint inflammation, which accelerates cartilage degradation and disrupts polysaccharides like hyaluronic acid (HA), chitosan, and chondroitine sulfate within the native extracellular matrix (ECM). A reduction in these molecules can weaken joint tissues [5], resulting in increased stiffness, swelling, and pain. In severe cases, this can lead to reduced lubrication, diminished mechanical support, impaired function, and ultimately to joint replacement surgery [6]. HA is a polysaccharide that plays a significant role as a lubricant and shock absorber; during ACLs, it is reduced in the synovial fluid (SF) due to increased hyaluronidase (HAS) and reactive oxygen species (ROS) activity.

Given the functional importance of such polysaccharides, several viscosupplementation and tissue engineering strategies for ACL injuries have been developed to restore the natural properties of articular cartilage [7–9]. Moreover, they are particularly appreciated for their biocompatibility, bioactivity and biodegradability, and greater stability compared to proteins like silk, gelatin, and collagen [19]. Among these options, intra-articular (IA) injections of HA [8,10] are one of the most effective methods for enhancing the impaired viscoelasticity of the SF, improving joint biomechanics, and protecting cartilage structure [9,11,12]. Despite its advantages, current HA treatments have some limitations, including a short duration within the joint, the requirement for multiple injections, inadequate rheological and physico-chemical properties, and sometimes adverse events (such as pain and reactions at the injection site) [13–15].

To address these challenges, new methods have been developed to chemically modify HA formulations. In particular, cross-linking reactions have been employed to increase HA's half-life and enhance its residence time, resulting in improved health benefits [16,17].

In addition to viscosupplementation strategies, other treatment options for ACLs have focused on inhibiting inflammatory-catabolic processes and improving chondroprotection. Advances in this field include the local IA administration of anti-inflammatory drugs, maximising drug effect directly at the site of action and minimizing their systemic side effects [18,19]. Several approaches have combined HA (or other hydrogels) with drugs such as dexamethasone [20] and ketoprofen [21]. In this context, natural compounds have been explored as potential therapeutic alternatives to drugs due to their pleiotropic biological effects along with a safer profile [22–24]. However, the combination of hydrogel with nutraceuticals has only recently emerged. Glucosinolate (GLS)-based products, derived from cruciferous vegetables, first emerged for their potential applications in cancer prevention. Then, evidence of their anti-inflammatory and antioxidant effects revealed broader benefits, particularly in chronic conditions [25], including certain musculoskeletal disorders [26,27]. The benefits of oral GLS administration have historically been ascribed to their highly active breakdown products, isothiocyanates (ITC), which are produced by the enzymatic action of plant myrosinase or gut bacteria [26,28,29]. In the context of ACL injuries, GLS hydrolysis products showed the ability to prevent cartilage destruction and chondrocyte degeneration [30,31].

Despite their potential, several limitations of ITC have been described. First, the metabolism rates of GLSs to ITCs vary among individuals [32], and they also respond differently to ITCs [32]. Additionally, ITCs may interfere with the pharmacokinetics of other drugs [33], have low stability due to their hydrophobic nature [34], and display high reactivity in active microenvironments, such as those found in ACLs. This reactivity can potentially generate ROS, exacerbating oxidative stress and inflammation. Moreover, ITCs may lose effectiveness under various conditions [35], partly because of their volatile nature [36].

The evidence for a direct active role of GLSs in exerting health benefits is growing [37–45], highlighting the potential to exploit their inherent activity as safer molecules in comparison to their breakdown products (ITCs). In this context, it is essential to note that, unlike ITCs, which are more easily distributed throughout the body [30], GLSs have a limited ability to reach human tissues upon oral administration. GLSs are hydrolysed into metabolites by myrosinase in the upper gastrointestinal tract or may transit to the colon (particularly if cooked cruciferous vegetables are ingested), where they are further hydrolysed by the resident microflora [39]. Hence, the development of novel delivery systems that can provide proper biologically active concentrations of GLS at the site of injury is crucial for addressing this significant challenge and offering innovative treatment options. This transition from a metabolite-centric perspective to an exploration of GLS action could enhance our understanding and boost the use of these compounds in clinical applications. Among various GLS-containing plants, those highly rich in benzyl-glucosinolate (BGL), also known as glucotropaeolin, an aromatic hydrophilic compound, have shown remarkable anti-inflammatory and antioxidant effects, potentially beneficial for arthritis [16,18,19,46].

This study aimed to use BGL as a representative active GLS to create a novel prototype of injectable GLS-releasing HA microstructured hydrogel with the goal to facilitate future therapeutic applications through the delivery of bioactive concentrations of BGL/GLS within the joint. In this preclinical in vitro study, we particularly aimed to assess both the safety and efficacy profile by examining BGL ability to inhibit inflammatory mechanisms and promote chondrogenic differentiation, key processes for promoting joint health and regeneration in vivo. To better mimic the joint microenvironment, we adopted resident joint cells and selected specific in vitro models to achieve reliable results that could maximize the translational potential of our findings. The formulation, designed to balance ease of injection and extended HA half-life, comprises BGL-loaded crosslinked HA microparticles dispersed in a non-crosslinked HA aqueous solution (Scheme 1). A comprehensive characterisation of the developed system and its components was conducted, including chemical, morphological, and rheological analyses, as well as the study of BGL release kinetics. Subsequently, the BGL-loaded microstructured HA underwent rigorous in vitro testing on human articular joint cells to assess its safety (by viability, cytotoxicity, and cell morphology tests) and efficacy (by assessment of anti-inflammatory activity and chondrogenesis). The general objective of this study was to boost the advancement of HA-based IA therapy, exploiting the anti-inflammatory and anti-catabolic properties of BGL, while offering an alternative strategy to oral supplementation of GLS.

2. Materials and methods

2.1. Synthesis of crosslinked HA microparticles (MP_{HA})

Crosslinked HA microparticles (MP_{HA}) were prepared by a water-in-oil (w/o) emulsion following a procedure described by Seong et al. [47] with some modifications. Briefly, HA powder (Hyaluronan sodium salt, Contipro a.s., Czech Republic, *MW*: 1000–1250 kDa) was dissolved in 0.25 M NaOH to obtain a 5% *w/v* HA solution. After complete dissolution, the crosslinker, 1,4-butanediol diglycyl ether (BDDE, ThermoScientific, Kandel, Germany) was added to the solution at different concentrations (1%, 4%, and 10% v/v), and the final mixture was emulsified in seed oil (6% v/v) on a magnetic stirrer at 1800 rpm for 48 h at 25 °C. At the end of the crosslinking reaction, the resulting microparticles (named $MP[x]_{HA}$ with x = 1, 4, or 10%) were vacuum-filtered several times with acetone to remove oil residues, followed by repeated washings with acetone-water gradient co-solvent and finally with pure distilled water. The $MP[x]_{HA}$ were centrifuged three times at 10000 rpm for 10 min and freeze-dried for 48 h. Preliminary chemical evaluations were performed on $MP[x]_{HA}$ to select the most promising % crosslinking before preparing microstructured hydrogels.

2.2. Preparation of BGL-loaded MP_{HA} (MP_{HA}-BGL)

BGL (PhytoLab GmbH&Co, Germany) was loaded into the MP_{HA} at

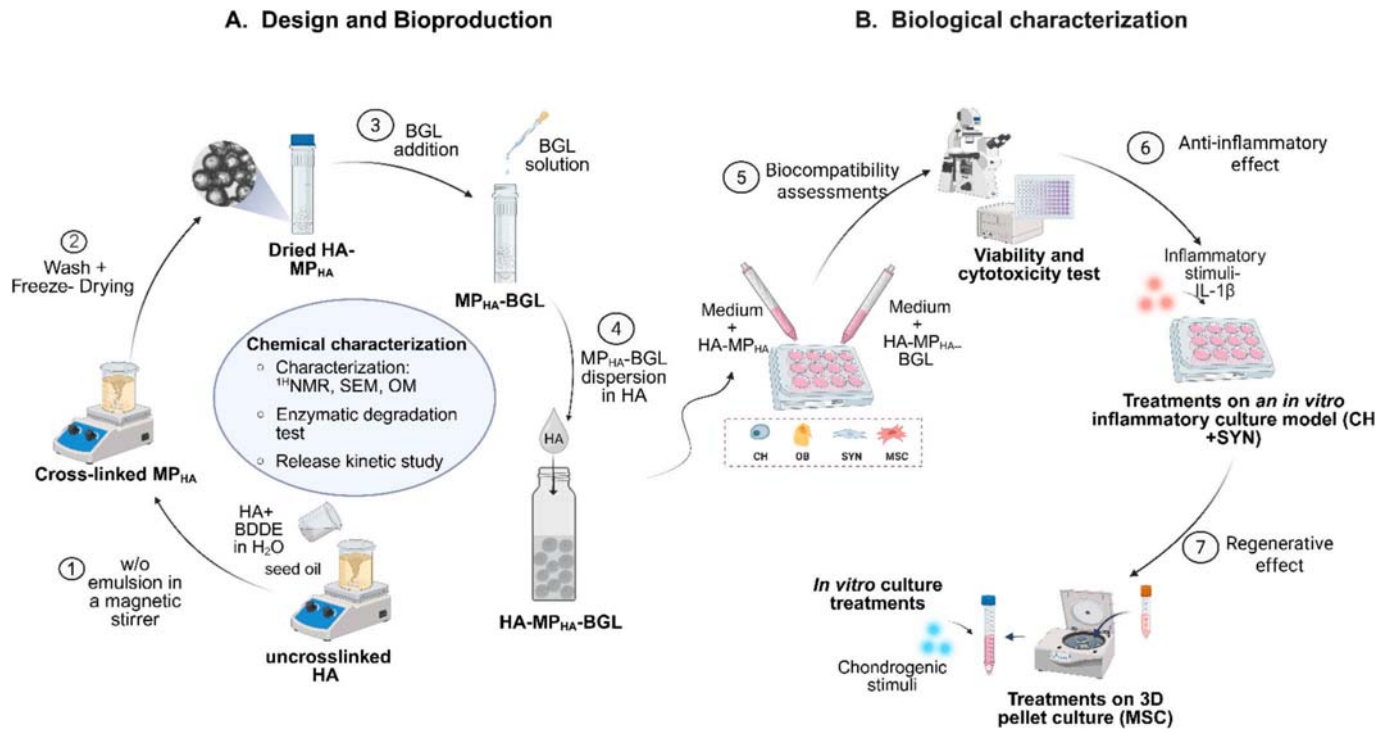

Scheme 1. Schematic flowchart that combines the chemical and biological characterisations of the developed microstructured injectable BGL-releasing hyaluronic acid (HA) for ACLs. **A**. Design and bioproduction: (1) synthesis of cross-linked microparticles (MP_{HA}); (2) production of dried MP_{HA}; (3) formation of microparticles loaded with BGL (MP_{HA}-BGL); (4) preparation of microstructured hydrogels (HA-MP_{HA}-BGL) by dispersion of microparticles in a non-cross-linked HA. **B.** Biological characterisation of HA, HA-MP_{HA}, and HA-MP_{HA}-BGL: (5) assessment of cytocompatibility on CH (chondrocytes), OB (osteoblasts), MSC (mesenchymal stromal cells), and SYN (synoviocytes); (6) evaluation of anti-inflammatory effect in co-culture systems with CH and SYN under interleukin beta (IL-1β) stimulation; (7) analysis of regenerative effect in 3D pellet cultures of MSC in terms of chondrogenic differentiation. HA: hyaluronic acid; NMR: nuclear magnetic resonance; SEM: scanning electron microscopy; OM: optic microscope; BDDE: 1,2-butanediol diglycyl ether; CH: chondrocytes; OB: osteoblasts; MSC: mesenchymal stromal cells; SYN: synoviocytes; w/o: water in oil. Created in BioRender. Velino C. (2025) https://BioRender.com/yld9iki.

two concentrations. At first, 520 μL of two stock solutions of BGL dissolved in ultrapure water (0.06 mg mL^{-1} and 0.12 mg mL^{-1}) were respectively added to 10 mg of dried MP_{HA} and gently mixed to let the particles swell and absorb BGL. BGL, absorbed by the microparticles, is stabilized within the HA matrix primarily through hydrogen bonding between the -OH groups of HA chains and -OSO_3^- and -OH groups of the BGL. BGL-loaded MP_{HA} (MP_{HA}-BGL) were then lyophilised for 24 h to eliminate the excess water and reconstitute the solid powder. Lyophilization ensured the stable retention of BGL molecules within the particles. According to this procedure, the nominal final concentrations of MP_{HA}-BGL were 0.31 wt% and 0.62 wt%.

2.3. Preparation of microstructured hydrogels

Preliminary evaluations were performed on different MP_{HA} concentrations (6.6%, 10%, and 20% *w/v*) dispersed in a 10 mg mL^{-1} aqueous solution of non-crosslinked HA to select the most promising in terms of rheological properties or cytocompatibility, before preparing microstructured hydrogel loaded with BGL. 10 mg mL^{-1} concentration was selected to obtain viscosities comparable to those found in HA formulations commonly used in clinical viscosupplementation [8,11]. These formulations were named HA-MP_{HA} 6.6%, HA-MP_{HA} 10%, and HA-MP_{HA} 20%, respectively. BGL-releasing microstructured hydrogels were further prepared by dispersing MP_{HA}-BGL (0.31 / 0.62 wt%) at 6.6% in a 10 mg mL^{-1} aqueous solution of non-crosslinked HA to obtain 5 μM and 10 μM BGL concentrations, named HA-MP_{HA}-BGL 5 and HA-MP_{HA}-BGL 10, respectively.

2.4. Enzymatic degradation tests

Tests of enzymatic degradation were carried out by placing the MP_{HA} in a shaking incubator at 37 °C for one week in a solution containing hyaluronidase 1 (HAS) enzyme (Hyaluronidase from bovine serum, 400–1000 U mg^{-1}, Sigma Aldrich) at two concentrations (10 U mL^{-1} and 100 U mL^{-1}). At predetermined time points (24 h, 48 h, 96 h and 1 wk), an aliquot of the solution was withdrawn to evaluate the particle morphology with optical microscopy and rheological analysis.

2.5. Loading efficacy and release kinetics tests

The evaluation of loading efficacy (*LE%*) and the release kinetics were conducted using a HA-MP$[1]_{HA}$ formulation loaded with a 0.62 wt % solution of Rhodamine B (RhB) as a model molecule. RhB was chosen due to its higher molar extinction coefficient compared to BGL, enabling sensitive detection even at low concentrations. Briefly, RhB-loaded MP$[1]_{HA}$ particles were placed in a modified open-ended Falcon tube. A 10 mg mL^{-1} HA solution was added to reconstitute a HA-MP$[1]_{HA}$.RhB 6.6% formulation. This tube was then placed inside a 50 mL Falcon tube containing 10 mL of 0.01 M PBS (pH 7.4). A cellulose dialysis membrane (14 kDa cutoff) separated the two solutions, allowing RhB exchange between the particle dispersion and PBS. This double-tube system was placed in a shaking incubator at 37 °C. At specific time intervals (30 min, 1 h, 2 h, 4 h, 6 h, 24 h, 48 h, and every wk, up to 7 wks), the PBS solution was analyzed by UHPLC-MS and replaced with fresh PBS.

2.6. Characterisation methods

Nuclear Magnetic Resonance (^{1}H NMR) spectroscopy (Bruker

Avance 600 MHz, Bruker, MA, USA) was used to determine the HA degree of modification (*MoD*), as an estimation of the crosslinking degree of the microparticles. Before the analysis, crosslinked MP[x]$_{HA}$ were hydrolysed in a 1 M HCl solution for 24 h at 60 °C, then freeze-dried for 24 h and finally dissolved in d_6- dimethylsulfoxide. The *MoD* was calculated by comparing the ratio of the relative peak integrals at $\delta = 1.5$ and $\delta = 1.77$, corresponding to the methyl groups of BDDE and the *N*-acetyl groups in HA, respectively, using Eq. (1):

$$MoD\% = \frac{\delta(1.5)/4}{\delta(1.8)/3} \times 100 \quad (1)$$

Scanning electronic microscopy (SEM) analysis was performed using a Leica/Cambridge Stereoscan 360 (Oxford Instruments, UK), with an accelerating voltage of 20 kV on gold-sputtered samples. Images were taken at 300× and 2000× magnification.

Optical microscopy (OM) images were captured using an Axioskop microscope (Zeiss, West Germany) to determine particle diameter before and after water absorption and calculate the swelling factor (*SwF)* by applying Eq. (2):

$$SwF\% = \frac{V_{wet} - V_{dry}}{V_{dry}} \times 100 \quad (2)$$

where V_{wet} and V_{dry} are the volumes of the wet and dried particles, respectively, calculated considering HA-MP$_{HA}$ spherical in shape. Image analysis was performed with the free software ImageJ (ImageJ 1.52a freeware) on more than a hundred particles, and values were calculated as the average value ± standard deviation.

Rheological characterisation was performed using an Anton Paar MCR102 rheometer (Anton Paar GmbH, Graz, Austria) with a 25 mm plate-plate configuration, keeping a plate-plate gap distance of 0.3 mm. The temperature was controlled by the integrated Peltier system and a Julabo AWC100 cooling system. The temperature varied from 25 °C to 37 °C, depending on the specific analysis. Amplitude sweep tests were performed at a fixed frequency of 1 Hz by increasing the deformation amplitude (γ) from 0.1% to 1000%. This test determined the viscoelastic properties (storage modulus: G'; loss modulus: G''). Viscosity (η) flow curves were obtained using the same instrumental set-up in a controlled shear rate mode. An increasing shear rate from 0.1 to 1000 s^{-1} was applied at 25 °C. Oscillatory Time sweep tests were performed at 0.5 Hz with a fixed deformation amplitude of 0.1%, both 3 min after hydrogel preparation (at 25 °C) and after its ejection from a 25-Gauge needle (inner diameter 16 mm) (at 37 °C). Measurements of G' and G'' were taken throughout. Similarly, rotational time sweep tests were performed at a constant shear rate of 0.1 s^{-1}, both after hydrogel preparation and after ejection from the needle, measuring viscosity. These experiments aimed to assess potential changes in hydrogel rheological properties during a simulated in vivo injection.

UHPLC−MS analyses were carried out on a Waters ACQUITY ARC UHPLC/MS (Milford, MA, USA) system consisting of a QDa mass spectrometer equipped with an electrospray ionization interface and a 2489 UV/Vis detector (the detected wavelength was 300 nm). The separations were performed on a Synergi Hydro column RP (4 μm particle size), 150 × 4.6 mm (Phenomenex, Torrance, CA, USA). The mobile phase was a binary mixture of H_2O (0.1% formic acid) and ACN (0.1% formic acid), and an isocratic elution (50:50, v/v) at the flow rate of 1.1 mL min^{-1} was applied. 10 μL of the sample solution was injected. Electrospray ionization was performed in a positive mode in the mass scan range 50–1200 Da, detecting the Q(+) ion at 443 *m/z*.

2.7. Isolation of articular joint cells

The in vitro experiments were conducted on human chondrocytes (CH), osteoblasts (OB), mesenchymal stromal cells (MSC), and synoviocytes (SYN) to explore the effects of our prototype on the primary cell types present in the joint. This approach aims to enhance the translational potential of our preclinical in vitro studies.

CH, OB, MSC, and SYN were isolated from the femur, tibial plateau, and synovium obtained from the clinical unit of the Rizzoli Orthopaedic Institution in accordance with the approval of the Ethics Committee (CE AVEC:34/2021/Sper/IOR; number: 0000929), and all participants provided informed consent before their inclusion in the study.

CH were isolated from the femur of articular cartilage through an enzymatic treatment. Briefly, cartilage fragments were enzymatically digested with 13.25 U mL^{-1} pronase (Sigma Aldrich) for 1 h at 37 °C and with 545 U mL^{-1} collagenase II (Sigma Aldrich) for 1 h and 30 min at 37 °C in an incubator in a humidified atmosphere with 5% CO_2. Cell suspension was cultured in Dulbecco's Modified Eagle medium (DMEM) (Fisher Scientific, Hampton, New Hampshire, US) with 10% fetal bovine serum (FBS) (Euroclone, #ECS5000L). OB and MSC were isolated from the tibial plateau, respectively, by mechanical and enzymatic isolation procedures and Ficoll gradient separation. Briefly, fragmented bone tissue was digested with 35.6 U mg^{-1} of collagenase P (Roche Diagnostics, Monza, Italy) and suspended in an isolation medium 'enzyme medium' (composed of Ham's F12 no calcium, DMEM no calcium, 25 μg mL^{-1} ascorbic acid, 100 U/100 μg Pen/strepto, 4 mM glutamine, and 2 mM calcium) for 2 h at 37 °C in a 5% CO_2 incubator. The bone chips were then cultured in Petri dishes (Corning, 100 mm; approximately 1 mL of bone per dish) with complete medium. Supernatants, containing MSCs, produced during mechanical isolation processes for obtaining bone chips, were then stratified on Ficoll (Cederlane) during centrifugation at 2500 rpm for 20 min. The resulting cell ring was collected, washed, centrifuged at 1600 rpm for 7 min, and cultured in α-MEM + 15% FBS supplemented with 0.05 g/500 mL penicillin G, and 25 μg mL^{-1} ascorbic acid. SYN were isolated from synovium through mechanical separation and cultured in OPTIMEM (Life Technologies Italia, Monza, Italy) with 10% FBS, supplemented with 100 U/mL penicillin-streptomycin, in a humidified atmosphere, at 37 °C with 5% CO_2. CH, SYN, MSC, and OB were maintained in culture with medium changes twice weekly and trypsinised with trypsin–EDTA solution upon reaching 90% confluence for subsequent biological assays.

2.8. In vitro studies on the cytocompatibility of HA-MP$_{HA}$ and HA-MP$_{HA}$-BGL: focus on several human joint cells

The cytocompatibility of microstructured hydrogels was evaluated at 24 and 72 h following the International Organization for Standardization (ISO) 10993-5:2009 Part 5 standard [48].

Direct contact tests were preferred due to the unique characteristics of the developed HA system, which made performing a conventional extract test unfeasible. However, to gain more indications on the potential toxic substances released from HA-MP$_{HA}$, we conducted a specific experiment using a reliable alternative option, the transwell system. In this setup, any leachable toxic substances from the system, placed in an insert above the cell monolayer, can diffuse through the porous membrane of the transwell and reach the underlying cells.

The cytocompatibility of the tested materials was assessed on four distinct primary human cell cultures (CH, OB, SYN, and MSC) to determine their overall biocompatibility with joint cells and their suitability for musculoskeletal applications. Joints are complex anatomical structures composed of multiple tissues, including cartilage, synovial membrane, and bone, each characterised by specific cellular compositions and biological functions. Because these tissues may respond differently to implanted materials, it is essential to assess biocompatibility across diverse cellular environments. This comprehensive approach helps minimize the risk of adverse reactions while boosting the translational potential for tissue regeneration and functional recovery.

This direct approach allowed us to gain valuable insights into cell interactions with the hydrogel as well as the biological responses (cell behaviour, adhesion, and proliferation). For the cytocompatibility assays, all cell cultures, at passage 2, seeded at a density of 4×10^4 cells per well in 48-well plates, were kept in culture medium at 5% CO_2 and

37 °C to allow the formation of a half-confluent monolayer to ensure adherence and progression to exponential cell growth. Subconfluency and cellular morphology were verified before initiating the treatments. The culture medium was carefully removed and discarded, and the selected treatments were added in a final volume of 500 μL, ensuring complete coverage of the cell monolayer. Regarding the microstructured hydrogels, the non-crosslinked HA matrix was transparent at the optical microscope, while the MPs were well visible as round materials with different cell coverage depending on their concentration (6.6% and 20% *w/v*). Simultaneously, negative and positive controls, including untreated/healthy cells (CTRL) and cells treated with 0.1% Triton™ X-100 (Sigma Aldrich, St. Louis, MO, USA) (TRY; as dead cell controls), were prepared. Cell cultures were exposed to sample materials and analyzed at two time points: 24 and 72 h.

2.8.1. Qualitative assessments of cytocompatibility

For qualitative evaluation, the interaction between cells and HA-MP_{HA} or HA-MP_{HA}-BGL was observed with an inverted and fluorescence microscope, focusing on examining general morphology, cell viability and the absence of cell reactivity around and in direct contact with the tested hydrogels.

Alterations in cell morphology were assessed by qualitative morphological grading of cell reactivity performed with and without metachromatic staining with toluidine blue (TB) at the inverted microscope (Nikon Eclipse 90i). For TB staining, cells were incubated with a 0.1% TB solution (Sigma-Aldrich) for 30 s at RT, followed by three washes with PBS-1x. Morphological and reactivity grading were assessed according to ISO 10993-5:2009, reporting a grade from 0 (no morphological changes and reactivity) to 4 (severe morphological changes and reactivity). Moreover, qualitative assessment of cell viability was performed with a Live/Dead (L/D) assay (Invitrogen, Waltham, MA, USA) and neutral red uptake (NRU) test. Regarding the L/D assay, cells were incubated with calcein-AM/ethidium bromide working solution and then examined at the inverted fluorescent microscope. Fluorescein isothiocyanate (FITC) and tetramethyl rhodamine (TRITC) filters were used to assess the live (green staining) and dead (red staining) cells, respectively. NRU test exploits the ability of cells to incorporate this dye into their lysosomes [49]. After a washing step with PBS-1x, cells were incubated with a 1.6% NR solution at 37 °C with 5% CO_2 for 30 min and then monitored and captured at the inverted microscope.

2.8.2. Quantitative assessments of cytocompatibility

Quantitative evaluations included the assessment of cell proliferation, inhibition of cell growth, and increase in cell death. In accordance with the ISO 10993-5:2009 guideline, a reduction of cell viability greater than 30% was considered indicative of cytotoxicity. After 24 and 72 h incubation, the culture medium was used for the LDH assay, and 400 μl of the appropriate assay-specific solutions were added to the cell monolayer, according to the specific assay protocols (Alamar blue and NRU tests). In particular, cell metabolism was evaluated with the Alamar Blue assay, using Alamar Blue™ Cell Viability Reagent (Invitrogen, Thermo Scientific, Waltham, MA, USA) diluted 1:10 in culture medium and incubated at 37 °C with 5% CO_2 for 4 h. Absorbance measurements were performed at 570 and 600 nm with the TECAN Infinite® 200 PRO microplate reader (Tecan Italia S.r.l., Cernusco Sul Naviglio, Italy). Cytotoxicity was also evaluated by measuring enzyme release from cell cultures using a lactate dehydrogenase (LDH) assay kit (Roche, Mannheim, Germany). Following the manufacturer's instructions, 100 μl of supernatants from both control and experimental groups were incubated with the working solution containing the dye for about 20 min at RT, followed by stop solution addition and, finally, absorbance was read at 492–620 nm with a TECAN microplate reader. Moreover, early cytotoxicity was assessed by the NRU test followed by the NR dye extraction (extraction solution composed of 49% deionized water, 50% absolute ethanol and 1% glacial acetic acid) and absorbance quantification (540 nm) with a TECAN microplate reader.

2.9. In vitro studies on the anti-inflammatory and regenerative potential of HA-MP_{HA}-BGL

The efficacy of microstructured hydrogels was evaluated in specific in vitro models that mimic the joint microenvironment, considering the multifaceted aspects of OA that affect cartilage repair. This evaluation focused on three key aspects: the hydrogel anti-inflammatory properties, pro-chondrogenic effect, and anti-catabolic actions. By addressing these interconnected factors, this study aimed to provide a comprehensive understanding of how microstructured hydrogels could facilitate cartilage repair in the ACL setting.

2.9.1. Effect of HA-MP_{HA}-BGL on inflammation

To evaluate anti-inflammatory activity, an in vitro model of inflammation was set up by co-culturing human CH and SYN at a ratio of 3:1 in a 24-well plate using a total volume of 1 mL (total number of cells seeded 16×10^4). The cultures were maintained in DMEM medium at 37 °C with 5% CO_2. After 24 h from cell seeding, the co-cultures were stimulated with interleukin 1 β (IL-1β) at a concentration of 10 ng mL^{-1} (Cell Guidance Systems, Cambridge, UK) and treated or not with HA-MP_{HA}.BGL 5/10 up to 7 days. The co-cultures of CH and SYN stimulated with IL-1 β represented the control group. All samples were observed with the inverted microscope and acquired to detect any signs of cytotoxicity. Supernatants from the co-cultures were collected to assess cytotoxicity through the LDH test, as detailed in the section on cytocompatibility. Cells were harvested for analysis with the quantitative reverse transcription-polymerase chain reaction (qRT-PCR). In particular, RNA was extracted from co-cultures using RNA pure solution (Euroclone, Milan, Italy), treated with DNase I (DNA-free Kit, Ambion, Austin, TX, USA) and then reverse transcribed using SuperScript™ VILO™ cDNA Synthesis Kit (Life Technologies) on 2720 Thermal cycler (Applied Biosystem, Life Technologies) at 25 °C for 10 min, 42 °C for 60 min, 85 °C for 5 min, and 4 °C for 30 min. Forward and reverse primers for the PCR amplification of key inflammatory markers are detailed in Table S2 and include nuclear factor kappa-light-chain-enhancer of activated B cells (NFKβ), induced nitric oxide synthase (iNOS), interleukin 6 (IL-6), Monocyte Chemoattractant Protein-1 (MCP-1), and cyclooxygenase-2 (COX2) - as well as two critical catabolic markers, metalloproteinase 13 (MMP-13) and A Disintegrin And Metalloproteinase With Thrombospondin Motifs 5 (ADAMTS-5), which are highly expressed in OA. SYBR Premix Ex Taq (TaKaRa Biomedicals, Tokyo, Japan) was used for Real-Time PCR, that was run in a LightCycler Instrument (Roche Molecular Biochemicals) as follows: 1 cycle (activation) at 95 °C for 10 s; 40 cycles (amplification) at 95 °C for 5 s (denaturation), at 60 °C for 20 s (annealing/extension); 1 cycle (melting curve) at 95 °C (denaturation), at 65 °C for 15 s (annealing), at 95 °C (extension); cooling 40 °C for 30 s. PCR products were relatively quantified with the comparative CT method, compared to the housekeeping mRNA expression of glyceraldehyde-3-phosphate dehydrogenase (GAPDH) (Table S2).

2.9.2. Effect of HA-MP_{HA}-BGL on chondrogenic differentiation

For chondrogenic differentiation, pellet cultures of expanded human MSCs (5×10^5 MSC/pellet) were first obtained through centrifugation at 1400 rpm for 7 min and then incubated at 37 °C with 5% CO_2 for approximately one week. These pellet cultures were then treated with HA-MP_{HA}-BGL while immersed in a 500 μl of chondrogenic medium (high-glucose DMEM (Gibco, Thermofisher Scientific, Monza, Milan, IT) with 50 mg mL^{-1} insulin-transferrin-selenium + premix (BD Biosciences, Franklin Lakes, New Jersey, US), 10% FBS, 10^{-7} M dexamethasone, 50 μg mL^{-1} ascorbate–2phosphate, 1 mM sodium pyruvate, and 100 U mL^{-1}–100 μg mL^{-1} pen–strepto, all from Sigma Aldrich) supplemented with the chondrogenic factors 10 ng mL^{-1} TGF-β3 (Cell Guidance Systems, Cambridge, UK). The culture medium and HA-MP_{HA}-

BGL were replaced twice a week, and pellet cultures were analyzed after 21 days. Samples were fixed with 4% paraformaldehyde (Sigma Aldrich) for 15 min at RT, snap-frozen in liquid nitrogen using the Tissue-Tek® optimal cutting temperature (OCT) compound (Sakura Finetech, CA, USA), and sliced into 10 μm sections with a cryostat. Sections were stained with Gill III Haematoxylin for 30 s at RT, rinsed in tap water for 10 min, and then stained with 0.1% safranin O for 3 min and 0.03% fast green for 5 min at RT to assess tissue architecture and proteoglycan content. Moreover, the safranin-O/fast green staining was semi-quantified using Bern's score, which is commonly employed to evaluate cartilage cultures and engineered pellets in vitro. This scoring method assesses specific parameters, including safranin stain, cell morphology and cell spacing, through a microscope (Nikon, Melville, NY, USA) [50]. The score ranges from 0 to 9, where a lower score indicates optimal chondrogenesis and a higher score suggests no chondrogenesis. Immunohistochemistry for type 1 collagen (COL1), type 2 collagen (COL2), type 10 collagen (COL10), MMP-13, and ADAMTS-5 was carried out with a colorimetric kit (Biocare Medical, Walnut Creek, CA, USA). Briefly, sections were incubated for 90 min at 4 °C with anti-human antibodies against COL1 (clone 5D8-G9, Sigma Aldrich, 5 μg mL^{-1}), COL2 (clone 6B3, Sigma Aldrich, 5 μg mL^{-1}), COL10 (Sigma Aldrich, 0.5 μg mL^{-1}), MMP-13 (R&D Systems, Minneapolis, MN; 5 mg mL^{-1}), and ADAMTS-5 (MyBioSource, 5 μg mL^{-1}). After three washes with PBS-1x, the sections were incubated with a multi-linker biotinylated secondary antibody and alkaline phosphatase-conjugated streptavidin for 20 min at RT (Biocare Medical, Pacheco, CA, US). Fast Red solution (Biocare Medical) was applied for colorimetric reactions, and the nuclei were counterstained with Gill III haematoxylin for 30 s at RT before being rinsed with tap water. Sections were evaluated under an Eclipse 90i microscope (Nikon), and microscopic fields (20× magnification) for semi-quantitative analysis were examined using the Hue/Saturation/Intensity system, with results expressed in percentages, where 100% represents maximum positivity and 0% denotes minimum positivity. Data of protein expression obtained by immunohistochemistry quantification were further analyzed by calculating specific ratios, usually adopted to evaluate cartilage quality, due to their ability to discriminate between healthy tissue (high COL2, low COL1, low MMP-13) and fibrocartilage or degenerated tissue (high COL1, high MMP-13 and ADAMTS-5). In particular, we examined COL2/COL1, COL2/COL10, COL2/MMP-13, and COL2/ADAMTS-5 ratios. The COL2/COL1 ratio was used to assess the chondrogenic differentiation, estimating a good chondrogenesis (high ratio) or fibrocartilage formation (low ratio). The COL2/COL10 ratio was used to provide insights into the progression toward a mature chondrogenic phenotype versus a hypertrophic state. COL2/MMP-13 and COL2/ADAMTS-5 ratios were used to give more information on the tissue neo-formed after chondrogenic differentiation, by measuring the balance between cartilage formation and degradation. Increased ratios of COL2/COL1, COL2/COL10, COL2/MMP-13, and COL2/ADAMTS-5 indicate a favourable environment for cartilage development and maintenance.

2.10. Statistical analysis and software

GraphPad Prism 10 software was used for statistical analysis. The Kolmogorov–Smirnov (K–S) test was used to assess data distribution. Outliers, checked by a ROUT (Q = 1%) test, were removed from each data set when present. Single-factor analysis of variance (ANOVA) was employed to assess the statistical significance of the results. We performed a two-way ANOVA and Dunnett's multiple comparisons test for analyses of biocompatibility (Alamar blue, LDH and NR) and effect (chondrogenesis and inflammation). $p < 0.05$ (*), $p < 0{,}01$ (**), $p < 0.001$ (***), and $p < 0.0001$ (****) were considered statistically significant.

3. Results and discussion

3.1. Influence of crosslinking on MP[x]$_{HA}$ swelling and rheology

The MP[x]$_{HA}$ were obtained using an inverse w/o emulsion by crosslinking HA with BDDE, selected for its better biodegradability and cytocompatibility compared to other crosslinkers [51]. Analysis of the peaks at 1.76 and 1.55 ppm in the ^{1}H NMR spectra (Figs. S1, S2, S3) allowed us to calculate the degree of modification (*MoD*) [94], whose values are reported in Table 1. The data show that the *MoD* lineraly increases with the amount of BDDE added during the crosslinking reaction.

The w/o microemulsion resulted in the formation of nearly perfectly spherical and homogeneous microparticles with a diameter in the range of 50–90 μm, as observed from both SEM and OM (Fig. 1, Table 1). According to Fig. 1 and Table 1, the amount of BDDE influences particle size, as higher crosslinker concentrations resulted in larger particles. To understand MP_{HA} behaviour in solution, the mean diameter distribution of dry and swollen particles was determined by OM both in water and in a 10 mg mL^{-1} HA solution, and the corresponding swelling factor (*SwF*) of the MP_{HA} were calculated (Fig. 1, Table 1). As evidenced by the mean diameter variations between dry and swollen MP[x]$_{HA}$ with different BDDE concentrations, a higher crosslinking degree resulted in less particle swelling (with the *SwF* of differently crosslinked samples being statistically different ($p < 0.0001$)). Additionally, all types of MP_{HA} swelled more in water than in the non-crosslinked HA solution ($p < 0.0001$). SEM micrographs provided a closer look at the MP[x]$_{HA}$ surface morphology: as expected, particle porosity was influenced by the amount of crosslinker used during synthesis (Fig. 1), with an increase in BDDE concentration that led to a pore size decrease.

Besides affecting the swelling behaviour, the crosslinking degree plays a crucial role in injectable materials, as it regulates the mechanical and rheological properties of the resulting microstructured-HA hydrogel. Amplitude sweep tests and viscosity flow curves were carried out to evaluate how the crosslinking degree impacts the overall mechanical response of the microstructured hydrogels, obtained by dispersing MP[x]$_{HA}$ in water at different concentrations (i.e. 6.6, 10, and 20% w/v, Fig. S4). The same tests were carried out for comparison on a non-crosslinked HA solution (10 mg mL^{-1}), which exhibited, as expected, an evident liquid-like behaviour (Fig. S5). As shown in the supporting information (Fig. S4), all the H_2O-MP[x]$_{HA}$ formulations exhibit gel-like behaviour (storage modulus $G' >$ loss modulus G''). The only exception is given by H_2O-MP[10]$_{HA}$ 6.6%, corresponding to the highest crosslinking ratio and the lower particle concentration, which displays a liquid-like behaviour ($G'' > G'$), likely due to MP poor swelling in an aqueous medium. G' and G'' were significantly affected by the extent of crosslinking. Specifically, the two moduli decreased by nearly two orders of magnitude from H_2O-MP[1]$_{HA}$ to H_2O-MP[10]$_{HA}$ across all tested particle concentrations. This trend can be attributed to the swelling behaviour of MP[x]$_{HA}$, as lower crosslinking leads to a higher swelling factor. Viscosity (η), on the other hand, showed a less pronounced variation with the crosslinking degree, with the most significant difference observed between H_2O-MP[10]$_{HA}$ and the other two formulations. When evaluating the effect of particle concentration on G', G'' and η, an overall increase in these parameters was observed with increasing MP[x]$_{HA}$ content. This effect was more pronounced for lower crosslinked particles (MP[1]$_{HA}$), which displayed the stiffest behaviour.

3.2. Effect of crosslinking degree on rheology

Two-component microstructured hydrogels were obtained by dispersing MP[x]$_{HA}$ at varying concentrations (6.6, 10, and 20% *w/v*) in a 10 mg mL^{-1} aqueous solution of non-crosslinked HA. This two-component system was designed to function as both a viscosupplement and a delivery system for GLS. HA was chosen as it is one of the main components of the AC and SF, thus it is considered an attractive

Table 1
Degree of modification (*MoD*), mean diameters (*D*) and Swelling Factor (*SwF*) in HA solution and H_2O of MP[*x*]$_{HA}$ with different crosslinker concentrations. Mean ± SD.

Sample	BDDE (% v/v)	*MoD* (%)	D_{dry} (μm)	$D_{wet\text{-}H2O}$ (μm)	$D_{wet\text{-}HA}$ (μm)	SwF_{H2O} (%)	SwF_{HA} (%)
MP[1]$_{HA}$	1	10.5	48 ± 10	204 ± 44	181 ± 40	74 ± 6	53 ± 7
MP[4]$_{HA}$	4	15.0	70 ± 14	242 ± 40	193 ± 34	57 ± 8	23 ± 4
MP[10]$_{HA}$	10	31.7	87 ± 17	247 ± 64	245 ± 26	24 ± 3	18 ± 7

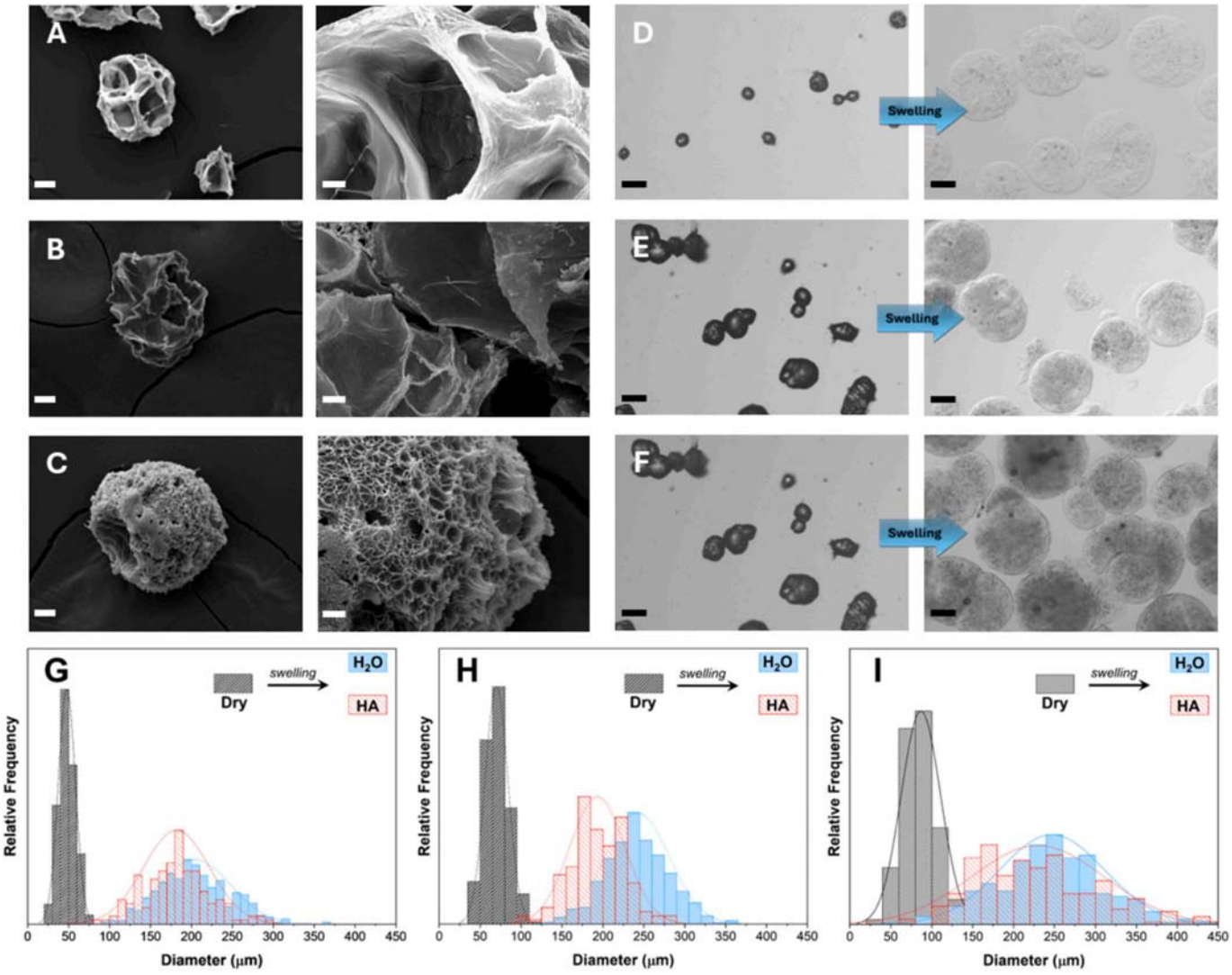

Fig. 1. Morphological characterisation of MP[*x*]$_{HA}$. (**A–C**): SEM micrographs of MP[1]$_{HA}$ (A), MP[4]$_{HA}$ (B), and MP[10]$_{HA}$ (**C**), at 300× (left) and 2000× (right); (**D–F**): OM photographs of MP[1]$_{HA}$ (**D**), MP[4]$_{HA}$ (**E**), and MP[10]$_{HA}$ (**F**), captured before (left) and after swelling (right) in HA solution. Scale bar: 15 μm (SEM 300×); 5 μm (SEM 2000×); 100 μm (OM pictures); (**G–I**): mean diameter distribution of dry and swollen particles in water (blue curve) and in HA (red curve) of MP[1]$_{HA}$ (**G**), MP[4]$_{HA}$ (**H**), and MP[10]$_{HA}$ (**I**).

material to develop tunable hydrogels for ACLs, being superior to other polysaccharides in terms of lubricating activity [52]. Understanding the physical properties and interactions within this two-component system is crucial for predicting its clinical outcomes in treating ACLs. Therefore, a thorough rheological characterisation was carried out to optimize the microstructured hydrogel formulation in terms of MP$_{HA}$ crosslinking degree and concentration, considering Hymovis®, a commercial HA hydrogel widely used in clinics [53], as a benchmark. The effect of MP[*x*]$_{HA}$ concentration is highlighted in Fig. S6 for HA-MP[1]$_{HA}$, HA-MP[4]$_{HA}$ and HA-MP[10]$_{HA}$. As expected, increasing particle concentration results in an increase in both G' and G''.

On the other hand, the effect of the crosslinking degree is reported in Fig. 2. When comparing particles with different crosslinking degrees added at the same concentrations to the HA solution, we observed that the highest G' values (Fig. 2, left column) were associated with the formulation containing the least crosslinked particles (HA-MP[1]$_{HA}$), consistent with the results obtained from the H_2O-MP[*x*]$_{HA}$ dispersion previously described in Section 3.1. In terms of viscosity (Fig. 2, right column), all tested hydrogel formulations display lower viscosities at low shear rates compared to the commercial product Hymovis®. Interestingly, as the crosslinking degree increases, the viscosity progressively decreases. This trend culminates in the sample HA-MP[10]$_{HA}$, which exhibits a viscosity similar to that of the non-crosslinked HA solution. Like Hymovis®, hydrogels exhibit a shear-thinning behaviour, where

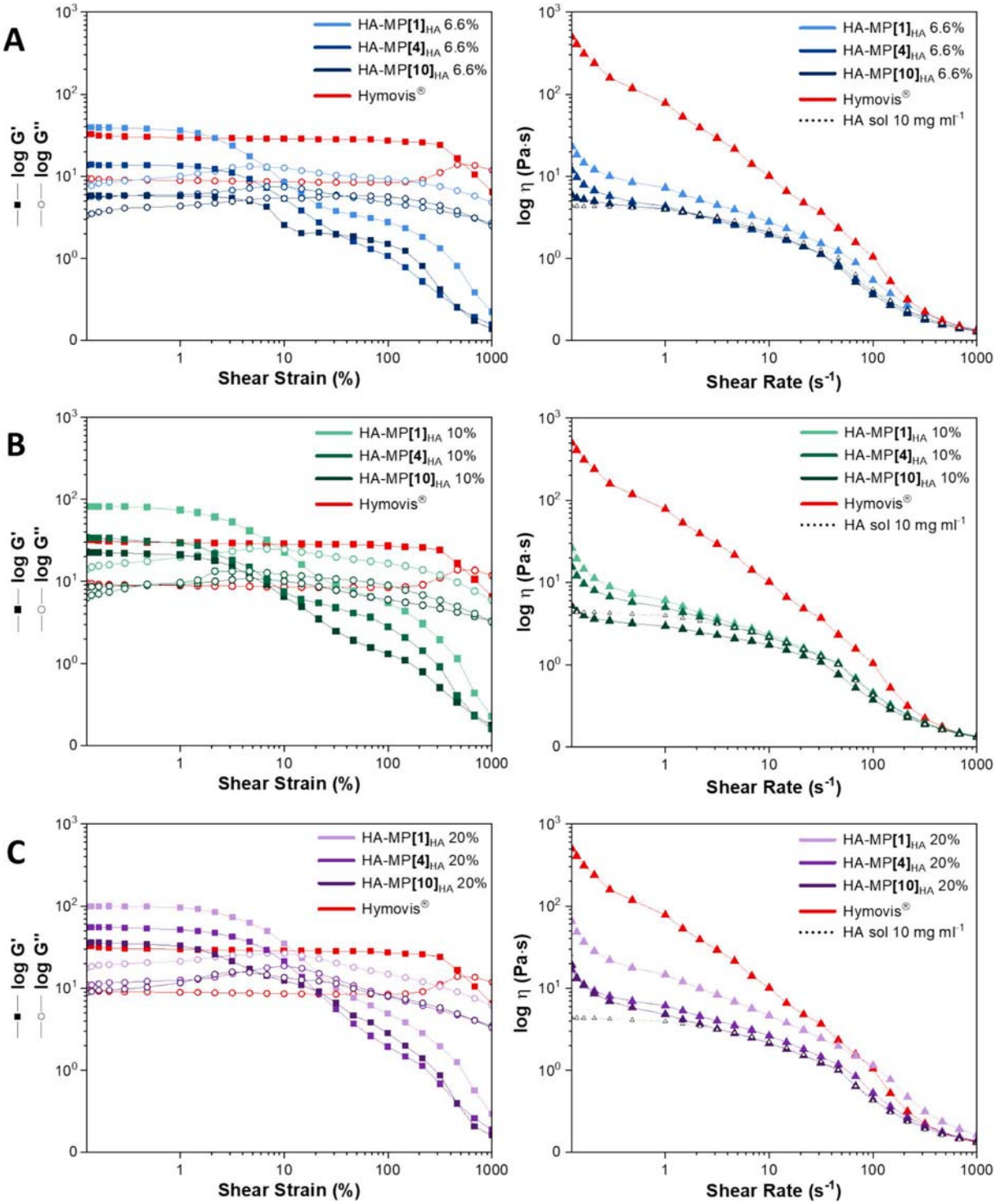

Fig. 2. Effect of MP_{HA} crosslinking degree on the rheological properties of microstructured hydrogels. Amplitude sweep tests (left) and viscosity flow curves (right) for HA-MP$[x]_{HA}$ formulations with varying degrees of crosslinking (x = 1, 4, 10) at **A**) 6.6% *w/v*, **B**) 10% w/v, and **C**) 20% w/v.

viscosity decreases with increasing shear rate. This non-Newtonian behaviour is crucial for injectable materials, as the high shear stresses encountered during injection cause a massive decrease in viscosity, thereby facilitating injectability. The enhanced characteristics of the two-component system are evident when comparing the rheological behaviour of the MP$[x]_{HA}$ with the same crosslinking degree and concentration dispersed in HA vs water (referred to HA-MP$[x]_{HA}$ and H_2O-MP$[x]_{HA}$, respectively): the soluble HA enhances the stiffness of the hydrogels by increasing both G' and G'' (Fig. S7), as well as the viscosity (Fig. S8), thereby proving the stabilizing effect of the HA matrix in the formulation.

Lastly, time sweep tests and rotational sweep tests (Fig. S9) carried out on HA-MP$[x]_{HA}$ at 6.6 w/v revealed that, when hydrogels are subjected to high shear stress that mimics injection conditions, they display good recovery of both G' and G'' (Fig. S9A) as well as of viscosity (Fig. S9B). This confirms the gel-like behaviour's preservation and the mechanical features' overall maintenance. Importantly, these findings indicate good injectable performance while retaining the desired

properties for functioning as a possible viscosupplement in the articular joint.

Rheological characterisation identified HA-MP[1]$_{HA}$, at all the concentrations tested, as the most promising candidate for an injectable viscosupplement. Among the tested formulations, it exhibited the highest G' and G'', indicating a strong and elastic material. Furthermore, HA-MP[1]$_{HA}$ displayed a higher viscosity than HA-MP[4]$_{HA}$ and HA-MP[10]$_{HA}$, suggesting its potential to effectively restore the impaired rheological and lubricating properties of the articular joint in ACLs. Additionally, it demonstrated good resistance to high shear stresses and a good recovery of its properties after a simulated injection. At low shear stresses, HA-MP[1]$_{HA}$ displays a lower viscosity than the commercial product Hymovis®, which could lead to a low perceived injection pain. Based on these combined properties, HA-MP[1]$_{HA}$ (hereafter referred to as HA-MP$_{HA}$) was chosen for further chemical and biological evaluation.

3.3. *In vitro cytocompatibility assessment of HA-MP$_{HA}$*

Several cytocompatibility analyses were carried out by direct methods, which are highly recommended to study any intended use of an implantable biomaterial in direct contact with the patient's tissue at long term [54]. In particular, we tested the least (HA-MP$_{HA}$ 6.6%) and most concentrated (HA-MP$_{HA}$ 20%) microstructured hydrogels, comparing them to the non-crosslinked HA solution (10 mg mL^{-1}), which served as a control group to test potential harmful effects after chemical modification.

Figs. 3A and 3B show the results of Alamar blue quantification, expressed as a percentage of proliferation compared to untreated cells (CTRL) at 24 h and 72 h post-treatment, respectively. This assay relies on metabolically viable cells to convert a substrate into a coloured product. As expected, treatment with TRY resulted in a significant decrease in cell proliferation ($p < 0.0001$). Interestingly, joint cells exhibited various responses in terms of proliferation to the two tested HA-MP$_{HA}$ concentrations. In particular, treatment with HA-MP$_{HA}$ 6.6% in all cell types tested did not reduce proliferation at both 24 and 72 h, similarly to the HA solution. Conversely, treatment with HA-MP$_{HA}$ 20% demonstrated a time-dependent reduction in cell proliferation compared to CTRL, but the effects varied among joint cells. Notably, OB showed an early decrease in proliferation by 34% ($p < 0.01$) at 24 h, which increased to 57% ($p < 0.05$) at 72 h. Conversely, HA-MP$_{HA}$ 20% did not significantly reduce cell proliferation in CH, SYN, and MSC at 24 h, yet it led to substantial decreases at 72 h, with reductions of 67% ($p < 0.001$), 58% ($p < 0.001$), 56% ($p < 0.05$) for CH, SYN and MSC, respectively. The mean values of proliferation inhibition observed after treatment with HA-MP$_{HA}$ 20%, exceeding 30% in OB at 24 h and in CH, OB, SYN and MSC at 72 h, suggest a potential cytotoxic profile for the highest concentration of MP$_{HA}$ microparticles, according to ISO 10993-5:2009 [55].

Assessments of the cell-biomaterial interaction using inverted microscopy and cell morphology with TB staining further supported Alamar blue findings, as reported in Figs. S10 and S11. HA and HA-MP$_{HA}$ 6.6% groups showed approximately 80–90% cell confluence and maintained a morphology and a metachromatic stain comparable to the CTRL, whereas the HA-MP$_{HA}$ 20% group showed lower cell confluence, low methacromatic stain and moderate morphological changes for all cell types, including enlarged cytoplasm, increased cytoplasmic processes, elongated shapes and release of small particles (Fig. S10). The microscopic analysis indicated a good interaction between HA-MP$_{HA}$ 6.6% and all cell types, which is critical for successful tissue engineering approaches (Fig. S11). In particular, we observed cell surface attachment to HA-MP$_{HA}$ 6.6% (indicated by M) with no cell lysis and reduction of cell growth, reporting a grade 0 of reactivity in accordance with ISO 10993-5:2009. In contrast, cells treated with HA-MP$_{HA}$ 20% exhibited some signs of morphological degeneration with different degrees of morphological and reactivity changes at 24 and 72 h and different cell sensitivity, especially at 24 h. In particular, we noticed in OB at 24 h, rounded cells and not more than 50% inhibition and reactivity zone limited to the area under specimens (grade 2), while CH, SYN and MSC displayed no cell lysis or round cells and only a slight non-significant inhibition of cell growth (grade 0). At 72 h, all cell types displayed moderate morphological and reactivity changes (grade 3), reporting rounded cells or lysed cells and approximately 60–70% growth inhibition and reactivity changes limited to the area under the specimen (grade 2). These characteristics reflect a clear reactivity, typically associated with a degeneration zone and lysis of cells around the tested biomaterials [55].

Overall, HA-MP$_{HA}$ 20% displayed changes in cell-biomaterial interactions, cell morphology, and metabolic activity, which may result from the cytotoxic effects of the material or from either alterations or injuries caused by the direct contact of cells with the microparticles. Notably, microparticles appear as dense, rounded structures, which hinder the visibility of the underlying cell layer; moreover, due to their heavier weight compared to the non-crosslinked HA, they do not remain in suspension; instead, they settle at the bottom of the well, creating varying coverage over the underlying cell layer based on the concentration used. In particular, when using HA-MP$_{HA}$ at a concentration of 6.6%, we observed that a significant portion of the cell monolayer was visible beyond the non-crosslinked HA. Conversely, when the HA-MP$_{HA}$ 20% system was employed, visualizing the underlying cell layer was challenging due to the near-complete coverage by HA-MP$_{HA}$ 20%. This observation led us to hypothesize that the inhibition of cell metabolism by HA-MP$_{HA}$ 20%, detected by the Alamar blue assay, may result from a reduced oxygen concentration caused by the extensive coverage of the monolayer cell culture by the microparticles dispersed in HA. Indeed, this feature can be attributed to the choice of in vitro direct contact methods, which are often more susceptible to mechanical damage and may also experience inadequate delivery of nutrients and oxygen/CO_2 to the cells, especially when using hydrogels [55].

To test this hypothesis, we performed a limited investigation involving HA-MP$_{HA}$ 20% treatment on each cell type, comparing the direct versus indirect contact method. In the indirect contact scenario, the HA system was confined within a transwell chamber, while the cells were placed at the bottom of the wells. These findings indicated that each cell type exhibited metabolic inhibition when in direct contact, whereas no inhibition was noted when in indirect contact, thereby supporting our hypothesis (Fig. S12).

To further ascertain the presence of cytotoxicity, we employed a comprehensive set of methods according to ISO 10993-5:2009. This approach was aimed at minimizing potential bias that could arise from relying on a single cytotoxicity assay, as no single test can definitely indicate cytotoxicity. The analyses were performed only at 72 h, which represented the time frame exhibiting the most significant metabolic impairments. Initially, we performed the LDH assay, which indicated no cytotoxicity for both HA-MP$_{HA}$ 6.6% and HA-MP$_{HA}$ 20% (Fig. 3C). The LDH assay is a widely recognized method for evaluating cytotoxicity by measuring the release of LDH enzyme into the culture medium following damage to the cell membrane. However, some authors have noted that the LDH test may be less sensitive than the NRU or MTT assays in detecting early cytotoxicity. Our results align with this evidence, prompting us to conduct further analyses to assess cell viability using two methods that are more sensitive to early toxicity: the L/D analysis and the NRU method (Figs. 3D, S13A). In particular, ISO standards regard lysosomal integrity, as detected by the NRU method, as a highly sensitive indicator of cell viability. The L/D assay confirmed the lack of cytotoxicity for HA-MP$_{HA}$ 6.6%, whereas some dead cells were observed after treatment with HA-MP$_{HA}$ 20% in CH, OB, and SYN (Fig. S13B). The NRU assay showed high viability (indicated by red positivity) of CH, OB, SYN, and MSC under all tested conditions, except for the control of cell mortality (TRY) and the treatment with HA-MP$_{HA}$ 20%, which displayed reduced NRU levels (Figs. 3D, S13A). The NR dye was extracted and quantified, showing a slight increase in viability after the treatment with HA-MP$_{HA}$ 6.6% for CH (14%), OB (22%), SYN (10%) and MSC (27%) compared to the CTRL. Conversely, treatment with HA-MP$_{HA}$ 20%

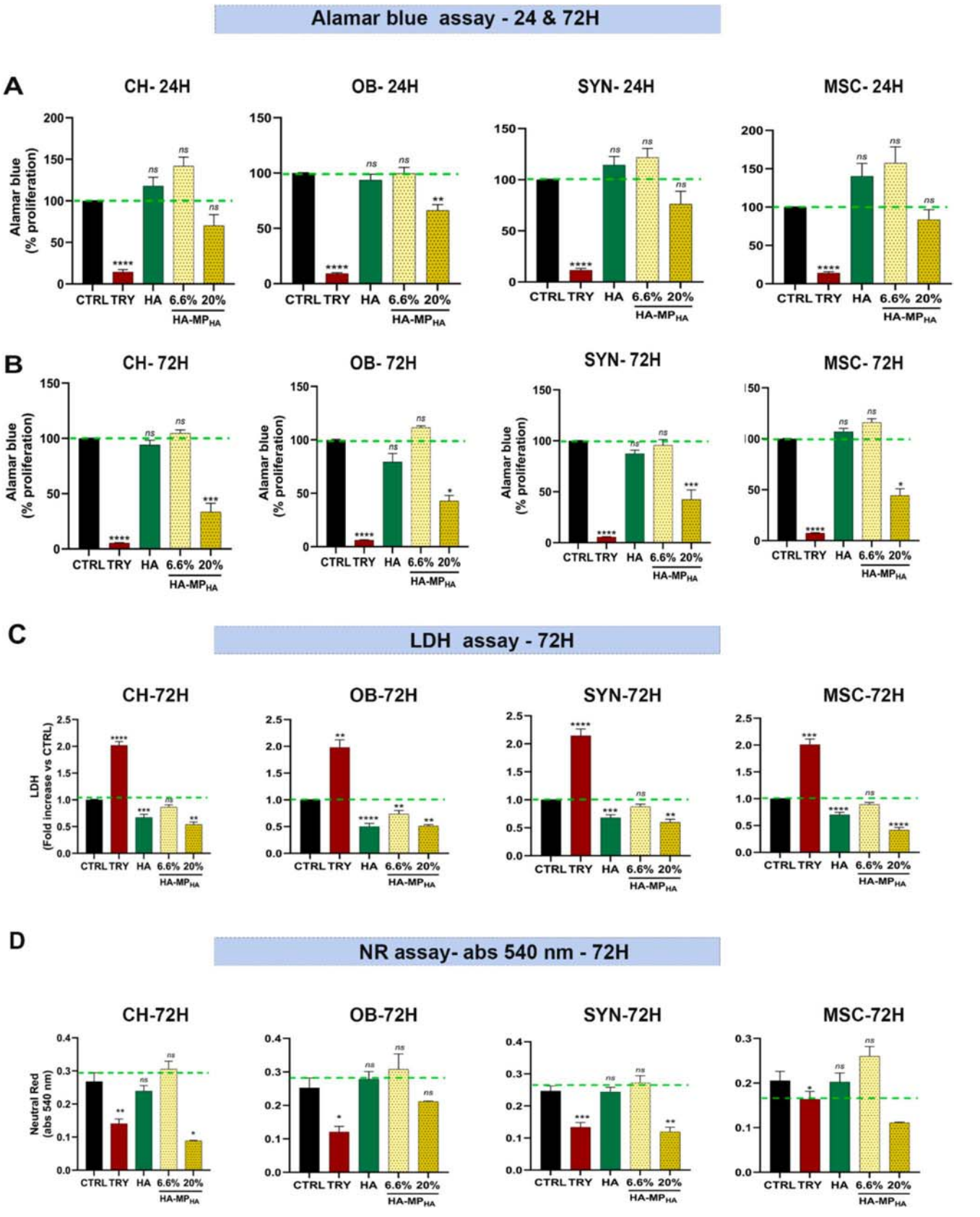

(caption on next page)

Fig. 3. Biocompatibility of HA and HA-MP_{HA} 6.6% and 20% on cells of the articular joint. **A–B**) Histograms of the metabolic activity assessed by Alamar blue test at 24 and 72 h for chondrocytes (CH), osteoblasts (OB), synoviocytes (SYN), and mesenchymal stromal cells (MSC) of untreated cells (CTRL), trytonX-100 treated (TRY), hyaluronic acid treated cells (HA), cells treated with crosslinked HA microparticles dispersed in a 10 mg mL^{-1} aqueous solution of non-crosslinked HA at 6.6% (HA-MP_{HA} 6.6%) and 20% (HA-MP_{HA} 20%). ****$p < 0.0001$: CTRL versus TRY in CH, OB, SYN and MSC at 24 and 72 h; **$p < 0.01$: CTRL versus HA-MP_{HA}- 20% in OB at 24 h; ***$p < 0.001$: CTRL versus HA-MP_{HA}- 20% in CH and SYN at 72 h; *$p < 0.05$: CTRL versus HA-MP_{HA}- 20% in OB and MSC at 72 h. **C**) Graphical representation of the cytotoxic activity assessed by the LDH test at 72 h for CH, OB, SYN and MSC of CTRL, TRY, HA, HA-MP_{HA} 6.6%, and HA-MP_{HA} 20% treated cells. ****$p < 0.0001$: CTRL versus TRY in CH and SYN at 72 h; **$p < 0.01$: CTRL versus TRY in OB at 72 h; ***$p < 0.001$: CTRL versus TRY in MSC at 72 h; ***$p < 0.001$: CTRL versus HA in CH and SYN at 72 h; ****$p < 0.0001$: CTRL versus HA in OB and MSC at 72 h; **$p < 0.01$: CTRL versus HA.MP_{HA} 6.6% in OB at 72 h; ****$p < 0.0001$: CTRL versus HA.MP_{HA} 20% in MSC at 72 h. **D**) Graphical representation of the Neutral Red (NR) absorbance at 72 h for CH, OB, SYN, and MSC of the CTRL, TRY, HA, HA-MP_{HA} 6.6%, and HA-MP_{HA} 20% groups. **$p < 0.01$: CTRL versus TRY in CH at 72 h; *p < 0.05: CTRL versus TRY in ON and MSC at 72 h; ***$p < 0.001$: CTRL versus TRY in SYN at 72 h; *$p < 0.05$: CTRL versus HA-MP_{HA} 20% in CH at 72 h; **$p < 0.01$: CTRL versus HA-MP_{HA} 20% in SYN at 72 h.

resulted in a significant decrease in viability (indicated by decreased red positivity) for CH (67%, $p < 0.05$) and SYN (52%; $p < 0.0001$) at 72 h, while showing a non-significant decrease for OB (16%) and MSC (46%). According to the ISO 10993-5:2009 standard [55], samples are deemed cytotoxic if the NR signal drops below to 70% of the CTRL [55]. Despite the observed decrease in viability, these data indicate the lack of cytotoxicity, with borderline values for CH. Collectively, our data indicate that the treatment with HA-MP_{HA} 6.6% is cytocompatible, similar to reference HA. In contrast, HA-MP_{HA} 20% showed decreased cell proliferation accompanied by some signs of early toxicity, characterised by lysosomal and nuclear damage, along with metabolic impairment, occurring before any permanent damage to the cell membrane. Based on these data, we selected HA-MP_{HA} 6.6% as the optimal condition for loading the GLS molecule, BGL.

3.4. Crosslinking-mediated stabilization of microstructured hydrogels against degradation

In vivo degradation of HA viscosupplements by HAS is a major concern in OA treatment, affecting their efficacy [112]. To this end, the HA-MP_{HA} 6.6% formulation was tested against enzymatic degradation to evaluate its response to HAS activity, by in vitro mimicking enzymatic degradation occurring in the articular microenvironment during OA [56]. Two HAS concentrations were selected based on degradation studies reported in the literature [57]. When incubated with HAS 10 U mL^{-1} (Fig. 4A–C) at physiological conditions (PBS, 37 °C), HA-MP_{HA} exhibited good stability in terms of morphological and rheological features for up to 96 h: the particles maintained their spherical shape during this time, and the rheological parameters (G', G'' and η) showed a

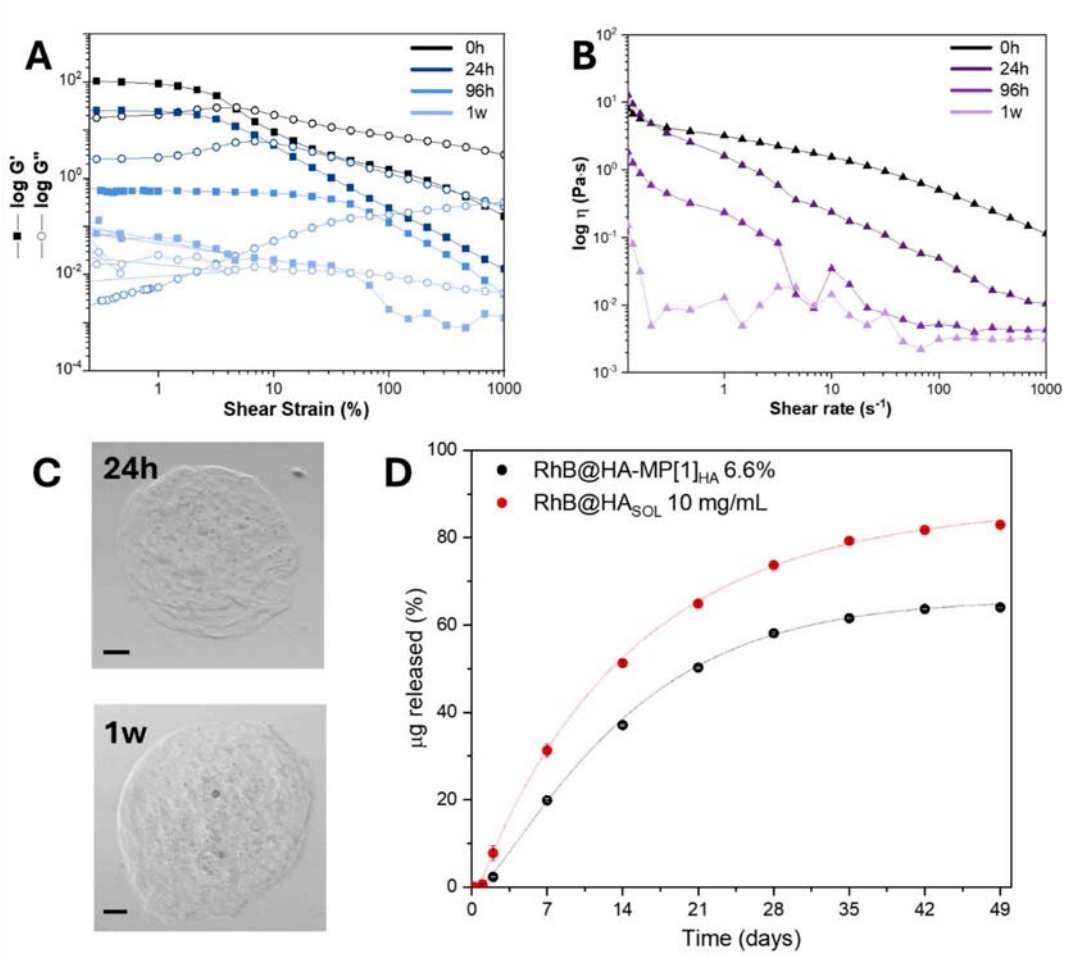

Fig. 4. **A**) Amplitude sweep test and **B**) viscosity flow curves measured after different times of enzymatic degradation of HA-MP_{HA} 6.6% system at HAS concentration of 10 U mL^{-1} (24 h, 96 h, and 1 week). **C**) Optical microscopy images of MP_{HA} at 24 h and 1 week (scale bar: 50 µm). **D**) Kinetic release profiles of RhB from the non-crosslinked HA solution (black curve) and the HA-MP[1]$_{HA}$ (red curve).

slight decrease, albeit their gel-like behaviour was preserved. However, after 1 week of incubation, a significant drop in both modulus and viscosity was observed. Since the particles remained intact (Fig. 4C), this suggests that the non-crosslinked HA matrix was primarily degraded by the enzyme. As expected, this effect was more pronounced at a higher enzyme concentration (100 U mL^{-1}) (Fig. S14). Here, the complete degradation of soluble HA occurred within 24 h, while particle degradation appeared to start only after 1 week. These results underscore the efficacy of crosslinking in stabilizing the material against enzymatic degradation, even at high enzyme concentrations. The greater resistance of HA-MP_{HA} to enzymatic degradation suggests a longer duration in the OA joint and more effective action than non-crosslinked HA.

3.5. RhB loading and kinetic release study

The feasibility of delivering a bioactive molecule via an injectable microparticle system offers the advantage of IA administration, thereby enhancing the functionality and bioavailability of the substance compared to oral delivery. Release profiles were obtained for two formulations: the first involved the direct loading of RhB as a model molecule within the 10 mg mL^{-1} non-crosslinked HA solution (HA_{SOL}), and the second involved RhB loaded within the $MP[1]_{HA}$ particles before dispersion in the HA solution (Fig. 4D). Consistent with previous observations, this particular formulation was chosen for its optimal rheological profile and demonstrated good cytocompatibility. Consequently, other formulations were not subjected to drug release testing in this phase. The release data for both formulations were fitted with the Weibull function, a commonly used empirical equation for describing drug release kinetics [58,59]. This model was chosen due to its flexibility in adapting to diverse release kinetics from complex matrices. The Weibull model provided an excellent fit ($R^2 > 0.999$, Table S1) for both RhB release profiles, revealing key differences driven by HA crosslinking. After 7 weeks of in vitro experiment, HA-MP_{HA} released ca. 62% of the encapsulated molecule while HA_{SOL} released ca. 82%. Additionally, the shape parameter (β) was higher for HA-MP_{HA} than for HA_{SOL} (suggesting swelling/erosion-controlled, sigmoidal release from the particles rather than a diffusion-driven process for the non-crosslinked solution). The lower maximum release and the $\beta > 1$ value for HA-MP_{HA} distinctly highlight the effective role of particle crosslinking in significantly retarding and modulating the release kinetics of the model drug compared to the simpler, faster release from the non-cross-linked solution. This gradual release is likely to occur in vivo, offering a promising approach to addressing the inflammatory characteristics of the OA microenvironment. Initially, this system can provide a rheological effect, and subsequently, it is expected to exert bioactive effects through the release of the BGL compound. This dual function could significantly enhance the treatment outcomes for OA.

3.6. Cytocompatibility assessment of HA-MP_{HA}-BGL 5 and HA-MP_{HA}-BGL 10

Assessing cell viability and activity is imperative for the future application of any developed biomaterial. To evaluate the safety profile of HA-MP_{HA} loaded with BGL at a concentration of 5 μM and 10 μM, we performed several in vitro direct contact analyses on articular cells, as detailed above. Including all these cell types is important for the translational relevance of our assays because, in vivo, IA delivery of this HA-MP_{HA}-BGL system will interact with these cells, directly contributing to its effectiveness in repairing ACLs. HA-MP_{HA} was used as a control group to assess the effects of the addition of BGL.

Fig. 5A shows the quantitative analysis of the proliferation rate with the Alamar blue test in the CTRL and experimental groups at 72 h. Treatment with HA-MP_{HA}-BGL 5 led to a slight decrease in the proliferation rate for most cell types compared to the control, except for MSCs. However, the average values of proliferation inhibition remained below the 30% threshold. This indicates that the delivery system used in our culture conditions lacks cytotoxicity, in accordance with ISO 10993-5:2009. Notably, HA-MP_{HA}-BGL 10 treatment resulted in a proliferation rate that was similar to the CTRL for CH and SYN, while OB and MSC exhibited higher values than the CTRL, though not statistically significant.

The microscopic analysis (Fig. 5B) and TB staining (Fig. S15) show cells morphology similar to CTRL cells and that cells adhered to HA-MP_{HA}-BGL 5 and 10 without displaying any signs of 'reactivity': no cell lysis and reduction of cell growth was detected, reporting a grade 0 of reactivity in accordance with ISO 10993-5:2009.

The cytotoxicity assay, measured by LDH levels and reported in Fig. 5C, indicated that HA-MP_{HA}, both alone and when loaded with 5 μM and 10 μM BGL, is not cytotoxic to any of the cell types tested. Of note, treatments with HA-MP_{HA}, HA-MP_{HA}-BGL 5, and HA-MP_{HA}-BGL 10 showed lower cytotoxicity values than the CTRL, reaching the most significant decrease in MSC ($p < 0.0001$). Results from the NRU assay, which evaluates the ability of live cells to incorporate NR in lysosomes, are shown in Figs. 5D and S16A. All cell types showed NRU in the lysosomal anionic sites, indicating cell viability, with particularly higher measurement values after the treatments with HA-MP_{HA}-BGL 5 and 10. However, HA-MP_{HA}-BGL 5 in CH showed a significant decrease ($p < 0.05$). Fig. S16B illustrates cell viability assessments using the L/D assay, where both the CTRL and experimental groups showed 95% of live cells with intact membranes, stained with a green dye and no red staining. These findings confirm the results obtained from the NRU test, reinforcing the biocompatibility and non-cytotoxicity of the HA-MP_{HA} and HA-MP_{HA}-BGL treatments.

From a biological view, using HA as a matrix and MP_{HA} as the encapsulation method for BGL creates a biomimetic environment that promotes positive cell responses. Specifically, both the HA-MP_{HA}-BGL 5/10 systems demonstrated a good cytocompatibility profile, showing optimal cell viability and no signs of cytotoxicity across all cell types, particularly for SYN and MSC, with no notable differences between the two doses. Although a slight inhibition of proliferation rate was observed at 24 h, remaining below 30%, all cell types showed an increased proliferation rate over the long term. This indicates no metabolic changes, consistent with the limits proposed by ISO-9001:2009.

3.7. Assessment of chondroprotection by HA-MP_{HA}-BGL

Recognizing ACLs as joint organ disorders characterised by a complex interplay of inflammatory and catabolic processes that result in joint degeneration and reduced capacity for cartilage regeneration, this study was specifically designed to evaluate the effects of HA-MP_{HA}-BGL in modulating processes associated with ACLs.

3.7.1. Assessment of anti-inflammatory effects by HA-MP_{HA}-BGL

To provide proof-of-principle for HA-MP_{HA}-BGL effectiveness in modulating inflammation, we established a co-culture of primary human CH and SYN under IL-1β stimulation. This co-culture model was preferred over monocultures of CH, as it better mimics the crosstalk between cartilage and synovium, which is crucial in regulating inflammation, offering a more reliable assessment of the potential effects of IA delivery of novel therapeutics. Exogenous stimulation with IL-1β was chosen as it is one of the master inflammatory cytokines implicated in arthritic joint damage and is highly expressed in osteoarthritic CH and SYN [5]. Here, we observed that treatments with HA-MP_{HA} and HA-MP_{HA}-BGL exerted an anti-inflammatory effect compared to IL-1β-stimulated control (Fig. 6). IL-1β-treated cells displayed a worse morphology than HA-MP_{HA} and HA-MP_{HA}-BGL-treated groups, suggesting a protective effect of HA-MP_{HA} both alone and in combination with BGL (Fig. 6A). To further assess their potential benefits on articular cell viability during inflammation, we conducted the LDH assay. Interestingly, this analysis revealed a significant decrease in LDH release after the treatment with HA-MP_{HA} ($p < 0.01$) and HA-MP_{HA}-BGL at both 5 and

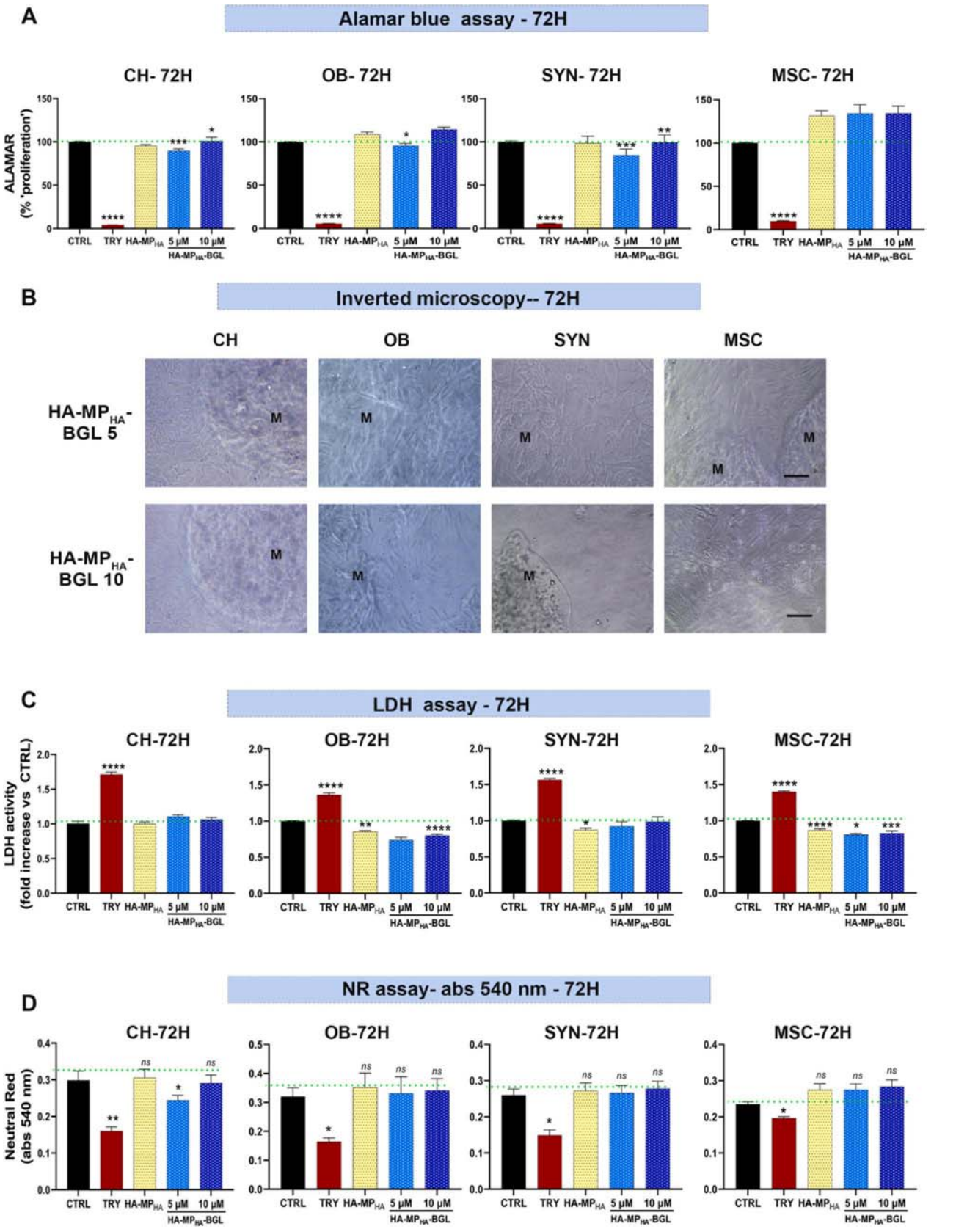

(caption on next page)

Fig. 5. Viability and cytotoxicity evaluations of HA-MP_{HA} 6.6%, HA-MP_{HA}-BGL 5 and HA-MP_{HA}-BGL 10 on cells of the articular joint. **A**) Histograms of the metabolic activity assessed by Alamar blue test at 72 h for chondrocytes (CH), osteoblasts (OB), synoviocytes (SYN), and mesenchymal stromal cells (MSC) of untreated cells (CTRL), trytonX-100 treated (TRY), hyaluronic acid treated cells (HA), HA-MP_{HA} 6.6%, HA-MP_{HA}-BGL 5 and HA-MP_{HA}-BGL 10. ****$p < 0.0001$: CTRL versus TRY in CH, OB, SYN and MSC at 72 h; ***$p < 0.001$: CTRL versus HA-MP_{HA}-BGL 5 in CH and SYN at 72 h; *$p < 0.05$ CTRL versus HA-MP_{HA}-BGL 5 in OB at 72 h; *$p < 0.05$ CTRL versus HA-MP_{HA}-BGL 10 in CH at 72 h; **$p < 0.01$ CTRL versus HA-MP_{HA}-BGL 10 in SYN at 72 h. **B**) Representative inverted microscopic images of HA-MP_{HA}-BGL 5 and HA-MP_{HA}-BGL 10 in CH, OB, SYN and MSC at 72 h. Scale bar: 50 μm (lower panel). **C**) Graphical representation of the cytotoxic activity assessed by LDH test at 72 h for CH, OB, SYN, and MSC of CTRL, HA-MP_{HA} 6.6%, HA-MP_{HA}-BGL 5 and HA-MP_{HA}-BGL 10 treated cells in the control and experimental groups. ****$p < 0.0001$ CTRL versus TRY in CH, OB, SYN and MSC at 72 h; **$p < 0.01$ CTRL versus HA-MP_{HA} in OB at 72 h; *$p < 0.05$ CTRL versus HA-MP_{HA} in SYN at 72 h; **$p < 0.0001$ CTRL versus HA-MP_{HA} in MSC at 72 h; ****$p < 0.0001$ CTRL versus HA-MP_{HA}-BGL 10 in OB at 72 h; ***$p < 0.0001$ CTRL versus HA-MP_{HA}-BGL 10 in MSC at 72 h. **D**) Graphical representation of the NR absorbance for CH, OB, SYN, and MSC in the control and experimental groups at 72 h. **$p < 0.01$ CTRL versus TRY in CH; *$p < 0.05$ CTRL versus TRY in OB, SYN and MSC; *$p < 0.05$ CTRL versus HA-MP_{HA}-BGL5 in CH.

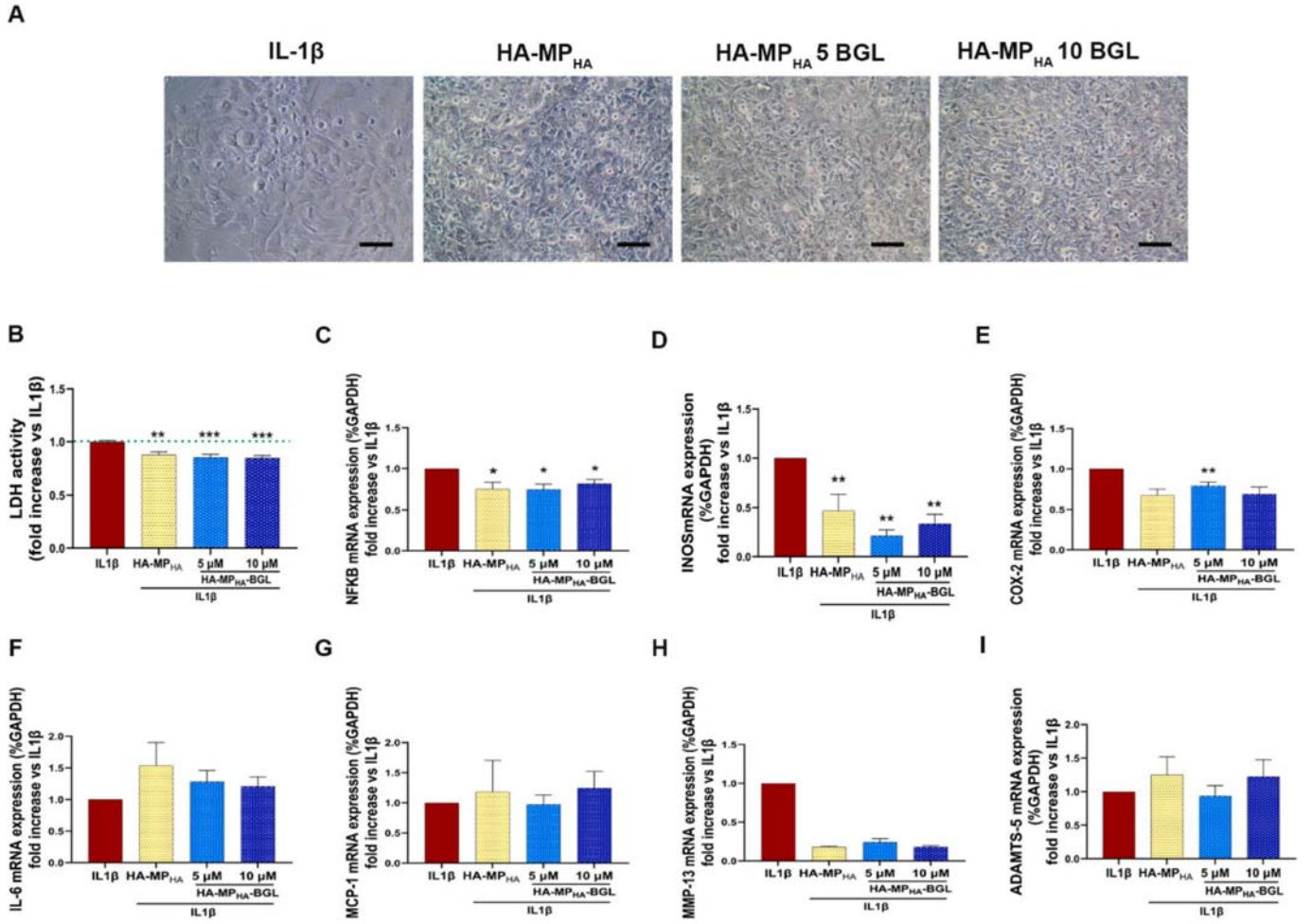

Fig. 6. Anti-inflammatory evaluations for HA-MP_{HA} alone and in combination with BGL 5 μM and BGL 10 μM in chondrocyte/synoviocyte co-cultures. **A**) Representative images of cell monolayers at inverted microscope at 72 h. Scale bar: 50 μm. **B**) Graphical representation of LDH activity. **C–I**) Graphical representation of mRNA expression (%GAPDH) expressed as fold increase vs IL-1β treatment of inflammatory markers NFkB, iNOS, COX-2, IL-6, MCP-1, MMP-13, and ADAMTS-5 in the IL-1β, HA-MP_{HA} and HA-MP_{HA}-BGL 5/10 treated groups. *$p < 0.05$: IL-1β versus HA-MP_{HA} and HA-MP_{HA}-BGL 5/10 for NFkB; **$p < 0.01$: IL-1β versus HA-MP_{HA}-BGL 5 for iNOS; **$p < 0.01$ IL-1β versus HA-MP_{HA} and HA-MP_{HA}-BGL 5/10 for iNOS; **$p < 0.01$: IL-1β versus HA-MP_{HA}-BGL 5 for COX-2.

10 μM concentrations ($p < 0.001$), compared to the IL-1β-stimulated control (Fig. 6B). Moreover, gene expression analysis showed a reduction in mRNA expression of NFκB ($p < 0.05$) and some of its downstream effectors (Fig. 6C–I). In particular, the most significantly downregulated gene was iNOS, which exhibited a 50% inhibition with HA-MP_{HA} and a 70–80% inhibition by HA-MP_{HA}-BGL at both 5 and 10 μM concentrations ($p < 0.01$). MMP-13 showed a marked inhibition of approximately 80% in response to each treatment, although this effect was not statistically significant. COX-2 exhibited a more modest inhibition (20–30%), achieving statistical significance solely for HA-MP_{HA}-BGL 5 ($p < 0.01$). Conversely, neither HA-MP_{HA} nor HA-MP_{HA}-BGL effectively inhibited the IL-1β-mediated activation of IL-6, MCP-1 and ADAMTS-5.

Overall, these data suggest a protective effect of IL-1β treatment by HA-MP_{HA}-BGL. Notably, plants known to contain BGL showed remarkable anti-inflammatory properties. Similarly, treatment with ethyl acetate fraction from the roots of *Brassica rapa* has been shown to inhibit pro-inflammatory mediators (including COX-2 and iNOS) through the suppression of NFkB in both an arthritis rat model and lipopolysaccharide-treated murine macrophages [76]. However, these preclinical studies did not determine whether the observed biological effects were exclusively attributable to BGL or its metabolite. Interestingly, our findings indicate that BGL within HA-MP_{HA} reduces the expression of some inflammatory markers, suggesting that it may partially mediate the beneficial effects of these extracts. Overall, these

results underscore the potential role of HA-MP$_{HA}$-BGL in influencing key biological mechanisms associated with joint degradation by modulating IL-1β-induced NFkβ signalling. Inhibiting inflammation at the early-stage of ACL is crucial for reducing the OA progression [5], potentially making this approach a 'safer' alternative to current oral anti-inflammatory drugs.

3.7.2. Assessment of chondrogenic effects by HA-MP$_{HA}$-BGL

In addition to addressing inflammation, enhancing the healing capacities of ACLs is another crucial factor in counteracting OA progression, as they do not heal spontaneously. Most treatment strategies focus on promoting chondrogenic differentiation to restore ACLs [60]. To date, there is no evidence directly linking the extracts of plants containing BGL or BGL itself to the promotion of cartilage regeneration. To thoroughly analyse the potential of HA-MP$_{HA}$-BGL 5 and 10 in promoting cartilage repair, we tailored our research to assess its ability to modulate MSC toward a chondrogenic phenotype. To this end, we used one of the most reliable models: MSC pellet which are recognized for their capability to activate signalling pathways that go beyond cartilage repair, enhancing cell-cell and cell-matrix interactions. As shown in Fig. 7A, treatment with HA-MP$_{HA}$-BGL 5 and 10 resulted in increased glycosaminoglycan content, as indicated by safranin O staining, and enhanced matrix organization, characterised by reduced cell density and more rounded cell shapes compared to the CTRL group. To more accurately assess cartilage differentiation, we employed a semi-quantitative measure of tissue repair based on Bern's score, which ranges from 0 (indicating no chondrogenesis) to 9 (indicating good chondrogenesis). The HA-MP$_{HA}$-BGL treatments at both 5 and 10 μM doses yielded higher Bern scores, indicating better chondrogenic differentiation compared to the CTRL ($p < 0.001$ and $p < 0.0001$, respectively), particularly with the highest BGL dose (Fig. 7B). All sub-parameters assessed for calculating the Bern score (cell morphology, matrix production and safranin-O) supported this trend, especially for the HA-MP$_{HA}$-BGL 10 treatment. Notably, the cell morphology parameter showed a significant difference between HA-MP$_{HA}$-BGL 5/10, with the 10 μM dose demonstrating superior outcomes (Fig. 7B).

Notably, most regenerative approaches often fail to achieve stable cartilage repair due to the undesired formation of fibrocartilage [61]. In our study, we examined a variety of immunohistochemical markers crucial for AC repair. This included extracellular matrix synthesis markers, such as COL2, fibrous and hypertrophic markers like COL1 and COL10, and catabolic markers, such as MMP-13 and ADAMTS-5. Fig. 7A indicates that cells treated with HA-MP$_{HA}$-BGL showed an increase in COL2 levels, with the highest expression observed following the HA-MP$_{HA}$-BGL 5 treatment ($p < 0.01$). As shown in Fig. S17, the positivity for this typical marker of the articular cartilage is mainly localized at the matrix level. Fig. 7C depicts an overall scenario where fibrous, hypertrophic, and catabolic markers were down-regulated after the treatment of MSC pellets with HA-MP$_{HA}$ and HA-MP$_{HA}$-BGL 5/10. Notably, immunohistochemical analysis revealed a decrease in COL1 expression, primarily located in the perinuclear area (Fig. S17) for both HA-MP$_{HA}$ and HA-MP$_{HA}$-BGL 5/10, with a significant reduction observed only for HA-MP$_{HA}$-BGL 5 ($p < 0.05$). Similarly, treatment with HA-MP$_{HA}$ at both 5 and 10 μM exhibited a significant reduction of COL10 in the MSC pellets, indicating a decreased tendency toward a hypertrophic state. When evaluating the two key catabolic markers involved in OA processes, we found that the HA-MP$_{HA}$ combined with 5 μM BGL ($p < 0.05$) was particularly effective in reducing the protein expression of these markers. Additionally, to gain more insights into the tissue formed after chondrogenic differentiation, we assessed various ratios of markers implicated in extracellular matrix-based differentiation and remodelling [62]. Fig. 7C indicates that treatment with HA-MP$_{HA}$ results in only a marginal increase in the COL2/COL1 ratio, while a more significant increase is evident after treatment with HA-MP$_{HA}$-BGL 5 ($p < 0.01$). Although the HA-MP$_{HA}$-BGL 10 did not show a statistically significant increase in the COL2/COL1 ratio, it displayed a tendency, similar to HA-MP$_{HA}$-BGL 5, to shift the balance toward a less fibrotic phenotype. In line with these findings, we noted that HA-MP$_{HA}$-BGL 5/10 down-regulated the COL2/COL10 ratio, indicating a reduced tendency of the neo-formed tissue to shift toward a hypertrophic phenotype. Furthermore, we tested the COL2/MMP-13 and COL2/ADAMTS-5 ratios to gain insights into matrix turnover in MSC pellets treated with HA-MP$_{HA}$-BGL 5/10. Interestingly, treatments at both doses were effective in lowering the degradation index in favour of cartilage synthesis, suggesting their potential to promote effective cartilage regeneration. Overall, these findings highlight that HA-MP$_{HA}$ treatments, akin to CTRL cells, effectively promote chondrogenic differentiation (as detected by COL2 expression), but at the meantime increase markers associated with fibrosis, hypertrophy and catabolism. Conversely, HA-MP$_{HA}$-BGL shifts the differentiation balance more favourably toward cartilage formation, resulting in a reduction of fibrotic, hypertrophic, and catabolic markers.

Notably, HA-MP$_{HA}$-BGL induced a simultaneous downregulation of MMP-13 and upregulation of COL2, both of which are well-established targets of the NFkB signalling pathway [63]. Given the previously discussed data on inflammation, these preliminary results suggest that HA-MP$_{HA}$-BGL may effectively inhibit NFkB activation, thereby exerting both anti-inflammatory and chondroprotective effects. Specifically, we found a direct downregulation of NFkB in CH and SYN. While we did not address NFkB expression during chondrogenesis of MSCs, we observed opposing changes in two key downstream targets of NFkB in MSC: downregulation of MMP-13 and upregulation of COL2 [63]. This data suggests a broad inhibition of NFkB by HA-MP$_{HA}$-BGL across various cell types from the joint microenvironment. Moreover, it is conceivable that the observed anti-inflammatory effects provide a favourable environment for chondrogenesis, reinforcing the dual role of HA-MP$_{HA}$-BGL in cartilage health.

3.7.3. Assessment of the combined effect of BGL and HA-MP$_{HA}$ on chondrogenic differentiation

After testing the chondroprotective and regenerative potential of the developed HA-MP$_{HA}$-BGL system, further investigations were aimed at determining whether the combined effects of BGL, MP$_{HA}$ and HA would be additive or synergistic in promoting chondrogenesis (Fig. 8). The initial assessment, utilizing the Bern score to evaluate histopathological outcomes, showed that BGL alone had significant chondrogenic effects ($p < 0.0001$). The HA-MP$_{HA}$ group exhibited significant improvements compared to the CTRL ($p < 0.0001$), suggesting that HA-MP$_{HA}$ may contribute positively to cartilage healing; however, the effects were significantly lower than those observed with BGL alone. The HA-MP$_{HA}$-BGL treatment showed similar values to BGL alone. This data suggests that the BGL is the dominant treatment influencing the morphological characteristics of chondrogenic differentiation, and its combination with HA-MP$_{HA}$ does not enhance or diminish its effects.

However, immunohistochemistry results revealed a synergistic effect of the combined treatment. Treatments with either HA-MP$_{HA}$ or BGL resulted in low COL2 levels, indicating chondrogenic differentiation similar to CTRL. In contrast, HA-MP$_{HA}$-BGL 10 (the combination of BGL with HA-MP$_{HA}$), significantly boosts COL2 expression compared to the HA-MP$_{HA}$ and BGL alone ($p < 0.01$). Similarly, COL1 expression demonstrated a synergistic interaction between BGL and HA-MP$_{HA}$. Indeed, both HA-MP$_{HA}$ and BGL alone decreased COL1 levels ($p < 0.01$); the combination (HA-MP$_{HA}$-BGL) showed lower levels than CTRL ($p < 0.001$).

Overall, these findings support the conclusion that combining BGL with HA-MP$_{HA}$ exerts synergistic effects, making this treatment strategy a promising candidate for intra-articular applications in cartilage repair. The results advocate for further exploration of the HA-MP$_{HA}$-BGL system in a clinical setting, given its potential to enhance cartilage repair and address degenerative joint conditions. These conclusions highlight the critical role of BGL in promoting chondrogenesis and underscore its therapeutic promise in regenerative medicine focused on cartilage repair.

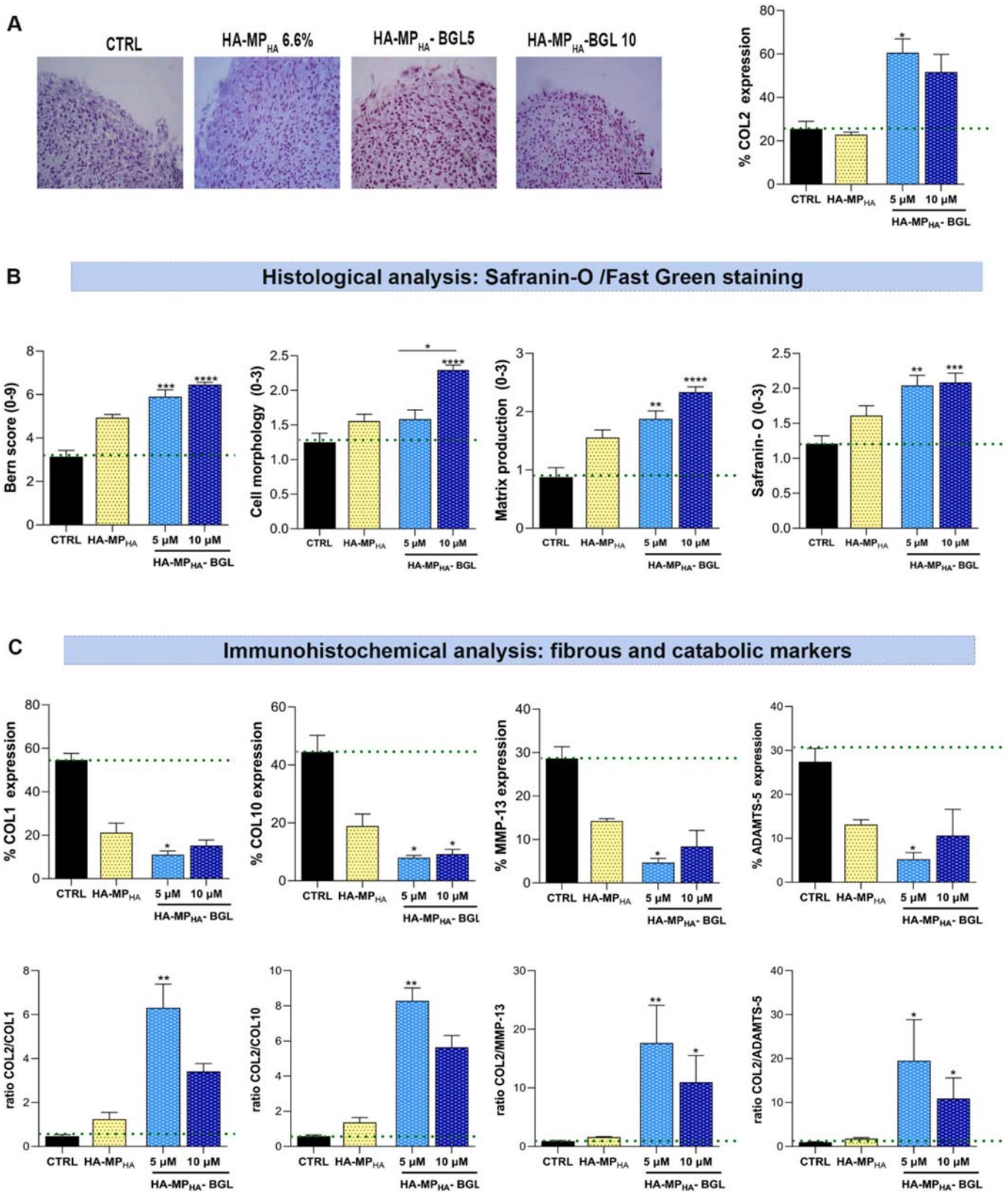

(caption on next page)

Fig. 7. Evaluation of the potential of HA-MP_{HA}-BGL 5 and 10 to promote chondrogenic differentiation and cartilage repair. A) Representative images: Safranin-O/Fast Green staining showing CTRL, HA-MP_{HA} 6.6%, HA-MP_{HA}-BGL 5 and 10 groups. Scale bar: 50 μm. Graphical representation of protein expression for COL2 in the control and treated groups. **B**) Histological analysis: graphical representation of the Bern score for histological evaluation, detailing sub-parameters such as cell morphology, matrix production and Safranin-O staining in CTRL, HA-MP_{HA}, and HA-MP_{HA}-BGL 5/10 treated groups. Statistical significance: ***$p < 0.001$: CTRL versus HA-MP_{HA}-BGL 5 for Bern score; ****$p < 0.0001$: CTRL versus HA-MP_{HA}-BGL 10 for Bern score. *$p < 0.05$: CTRL versus HA-MP_{HA}-BGL 5 for COL1 and COL2. **C**) Immunohistochemical parameters: graphical representation of typical fibrous (COL1), hypertrophic (COL-10) and catabolic (MMP-13 and ADAMTS-5) markers involved in cartilage degeneration, along with their ratios as compared to COL2 expression. Statistical significance: *$p < 0.05$: CTRL versus HA-MP_{HA}-BGL 5 for COL1; *$p < 0.05$: CTRL versus HA-MP_{HA}-BGL 5 and 10 for COL10; *$p < 0.05$: CTRL versus HA-MP_{HA}-BGL 5 for MMP-13 and ADAMTS-5. The lower panel depicts the ratios: COL2/COL1, COL2/COL10, COL2/MMP-13 and COL2/ADAMTS-5. Statistical significance: **$p < 0.01$: CTRL versus HA-MP_{HA}-BGL 5 for ratios COL2/COL1 and COL2/COL10; **$p < 0.01$: CTRL versus HA-MP_{HA}-BGL 5 for COL2/MMP-13 and *$p < 0.05$ for CTRL versus HA-MP_{HA}-BGL 5 for COL2/MMP-13; *$p < 0.05$ for CTRL versus HA-MP_{HA}-BGL 5 and BGL 10 for COL2/ADAMTS-5.

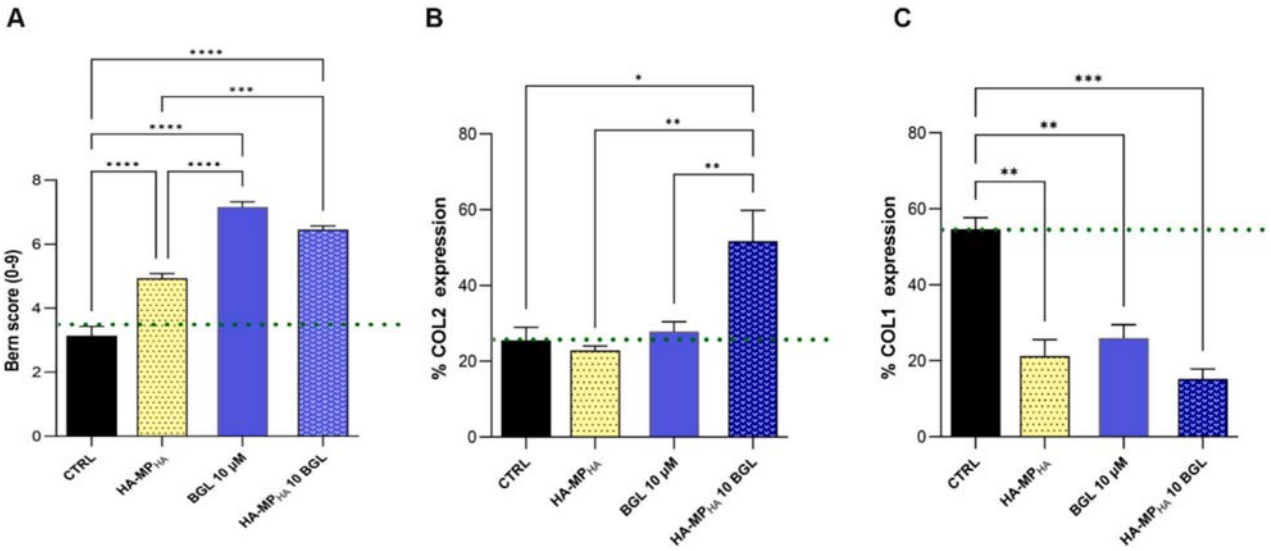

Fig. 8. Graphical representation of the Bern score (A), and protein expression for COL2 (B) and COL1 (C) in the 3D pellet cultures of mesenchymal stromal cells in the CTRL, HA-MP_{HA}, BGL 10 and HA-MP_{HA}- BGL 10 groups. *$p < 0.05$; **$p < 0.01$; ***$p < 0.001$; ****$p < 0.0001$. Ordinary one-way ANOVA, Tukey's multiple comparisons test.

3.8. Study limitations, strengths, and perspectives

The integration of material science with biologically relevant molecules marks a relatively recent advancement. Previous studies have combined HA hydrogels with drugs targeting biological pathways, demonstrating potential benefits for ACL repair [20]. Indeed, technological advances in chemistry and tissue engineering have led to innovative hydrogel-based delivery systems for AC repair [64–66]. Additionally, research is exploring novel hydrogel formulations that incorporate various molecules, including nutraceuticals. While much research on the bioactive effects of nutraceuticals has focused on oral administration, some studies are now exploring innovative combinations of hydrogels and nutraceuticals [67–71]. In this varied context, gaining a broader understanding of the clinical perspectives of nutraceuticals remains challenging. Our study aimed to validate the hypothesis that GLS incorporation into HA hydrogels confers multiple functional benefits, paving the way for novel injectable therapeutic options for ACLs. Our findings demonstrated that HA-MP_{HA}-BGL positively influences anti-inflammatory, anti-catabolic and pro-regenerative processes related to ACLs (Fig. 9).

This prompts further study of different GLS groups, including aliphatic, aromatic, and indole GLS, along with comparisons to their respective metabolites. However, validation in preclinical in vivo models is crucial to confirm effectiveness in a complex microenvironment compared to IA drug applications.

Future GLS applications via IA administration face detection challenges for minimal compound amounts. This study utilized a model molecule, rhodamine, to explore release kinetics. To enhance the reliability of our findings, we recommend that future studies focus on developing a specific and sensitive analytical method that can accurately detect BGL in release solutions without interference from surrounding factors. Also, examining different crosslinking degrees, particle concentrations, and lubrication conditions could improve the system's rheological and biological value.

To validate the positive effect of the HA-MP_{HA}-BGL system, our research was performed on several types of human primary cultures, thus enhancing its clinical relevance. Specifically, we extended our analysis to several primary human cell cultures from the articular microenvironment, including CH, OB, SYN, and MSC. This comprehensive methodology enabled us to assess the sensitivity of different human cell types to HA-MP_{HA}-BGL treatment, improving our capacity to predict cellular responses to IA delivery of HA-MP_{HA}-BGL, offering valuable insights into the therapeutic healing potential and highlighting different sensitivities among cell types, overall fostering the translational relevance of this study.

Preclinical in vivo studies on orally administered GLS have struggled to separate their effects from those of their metabolites, due to their rapid conversion to ITC at the gastric level. To clarify GLS's direct effects, myrosinase thioglucosidase-free in vitro models are essential. Our previous work demonstrated that both metabolites and their precursors are bioactive, particularly regarding osteogenesis [42]. This study reinforces such findings across various cellular processes, offering a valuable strategy to identify GLS's inherent properties in several musculoskeletal systems. Moreover, it also addresses limitations associated with GLS's slow adsorption and rapid metabolic conversion in the gut. A significant innovation of this study is the proposed IA administration, which aims to increase bioactive concentrations of GLS in joint tissues, thereby offering new therapeutic opportunities for ACLs.

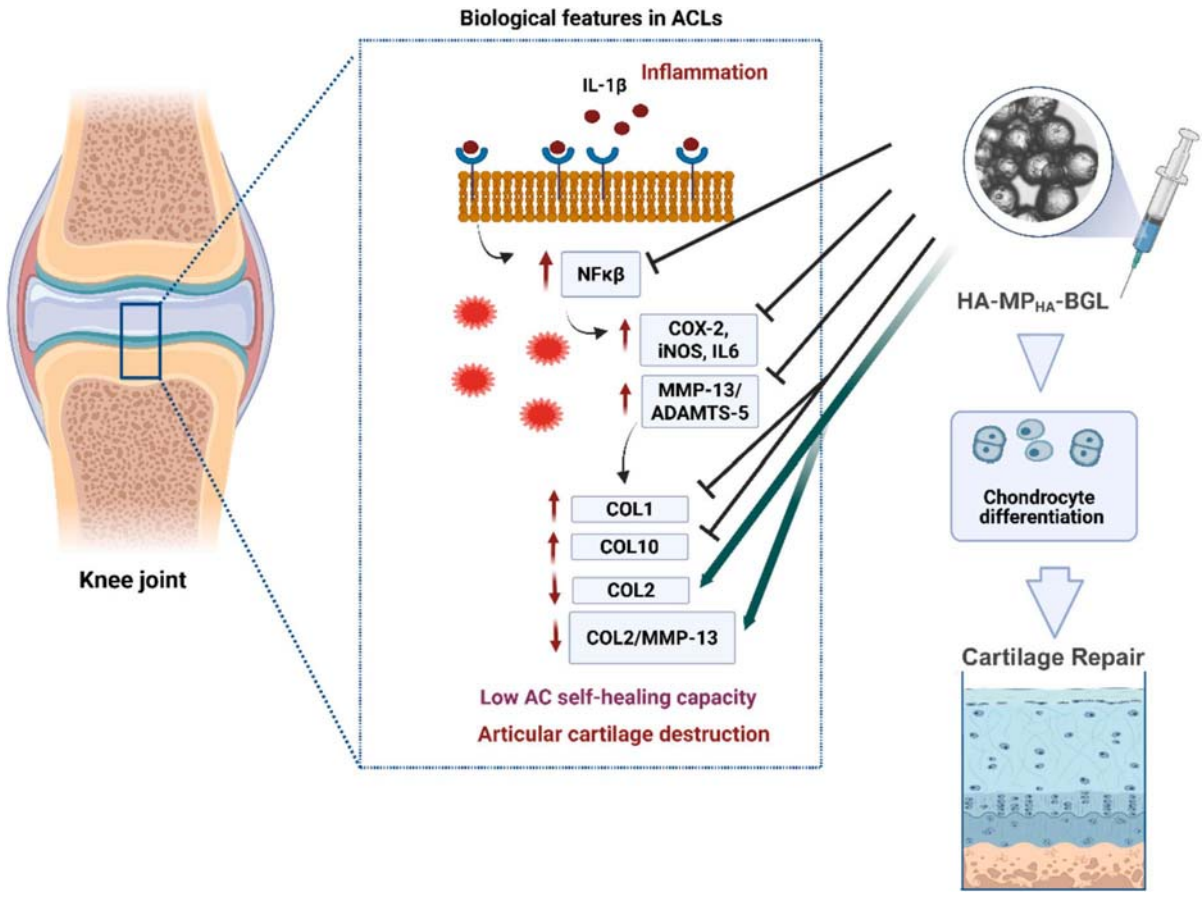

Fig. 9. Graphical scheme illustrating the overall anti-inflammatory, anti-catabolic and chondroprotective effect of HA-MP_{HA}-BGL. The upper part of the panel indicates that treatment with HA-MP_{HA}-BGL in the co-culture systems contributes to reducing typical inflammatory markers in CH and SYN: NFkB, COX-2, iNOS, IL-6, MMP-13 and ADAMTS-5. The lower part of the panel indicates that treatment with HA-MP_{HA}-BGL reduces typical fibrotic (COL1) and hypertrophic (COL10) markers while increasing a typical chondrogenic (COL2) marker and the ratio COL2/MMP-13 in the 3D pellet cultures of MSC. Green arrow: promotion; Black arrow: inhibition. Created in BioRender. Desando, G. (2026) https://BioRender.com/cit9n5p.

4. Conclusion

This study presents a novel method for loading GLS, particularly BGL, into a two-component HA matrix and conducted in vitro validations to assess its feasibility as an alternative IA strategy for treating ACLs. The primary challenge was to create a prototype that conjugates proper physicochemical properties with the ability to maintain cartilage tissue homeostasis, thereby enhancing AC repair following IA injection. MP_{HA}, prepared by oil emulsion technology, were able to effectively load and release the BGL in a prolonged way. HA-MP_{HA}-BGL, which comprises MP_{HA}-BGL (crosslinked MP_{HA} microparticles loading BGL) immersed in HA solution, demonstrated suitable injectability and chemical-physical properties for the IA viscosupplementation. In addition to its favourable biomechanical properties, this prototype exhibited good cytocompatibility with various cell types resident in the articular microenvironment, including CH, OB, MSC, and SYN. Notably, this study provided the first in vitro proof of principle of the chondroprotective effect of HA-MP_{HA}-BGL in promoting chondrogenesis and reducing inflammation, suggesting promising prospects for this novel approach in treating ACLs. Finally, this research provides benchmarks for the encapsulation and the preclinical testing of other GLS molecules to promote joint repair.

Abbreviations

AC	Articular cartilage
ACLs	Articular cartilage lesions
ANOVA	Analysis of Variance
BDDE	1,4-Butanediol Diglycidyl Ether
BGL	Benzylglucosinolate/glucotropaeolin
COX-2	Cyclooxygenase-2
CTRL	Control
CH	Chondrocytes
COL1	Type 1 collagen
COL2	Type 2 collagen
COL10	Type 10 collagen
DMEM	Dulbecco's Modified Eagle Medium
ECM	Extracellular Matrix
EE	Encapsulation Efficacy
FITC	Fluorescein Isothiocyanate
FBS	Fetal Bovine Serum
GLS	Glucosinolates
HA	Hyaluronic acid
HAS	Hyaluronidase
HPLC	High-Performance Liquid Chromatography
IA	Intra-articular
ITC	Isothiocyanates
ISO	International Organization for Standardization
iNOS	Inducible Nitric Oxide Synthase
LDH	Lactate dehydrogenase
L/D	Live and Dead
LE%	Loading efficacy (%)
MSC	Mesenchymal stromal cells
MMP	Matrix metalloproteinase

MoD	Degree of Modification
MP_{HA}	Hyaluronic acid-based microparticles
MW	Molecular Weight
NFkB	Nuclear factor kappa-light-chain-enhancer of activated B cells
NMR	Nuclear Magnetic Resonance
NRU	Neutral Red Uptake
NR	Neutral Red
OA	Osteoarthritis
OB	Osteoblasts
OM	Optical Microscopy
PBS	Phosphate-Buffered Saline
qRT-PCR	Quantitative reverse transcription-polymerase chain reaction
RhB	Rhodamine B
ROS	reactive oxygen species
SEM	Scanning Electron Microscopy
SF	Synovial Fluid
SwF	Swelling Factor
SYN	Synoviocytes
TB	Toluidine Blue
TRY	Tryton X-100
TRITC	Tetramethylrhodamine Isothiocyanate

CRediT authorship contribution statement

Laura Gambari: Writing – original draft, Visualization, Validation, Supervision, Methodology, Investigation, Funding acquisition, Data curation, Conceptualization. **Cecilia Velino:** Writing – original draft, Visualization, Validation, Methodology, Investigation, Funding acquisition, Data curation, Conceptualization. **Roberto Gotti:** Writing – review & editing, Methodology, Investigation, Data curation. **Luana Di Lisa:** Writing – review & editing, Methodology, Investigation. **Lucia Ferrazzano:** Writing – review & editing, Methodology, Investigation. **Dario Corbisiero:** Writing – review & editing, Methodology, Investigation. **Alessandra Tolomelli:** Writing – review & editing, Supervision, Investigation. **Alessandro Panciera:** Writing – review & editing, Methodology, Investigation. **Cesare Faldini:** Writing – review & editing, Methodology, Investigation. **Alberto Ruffilli:** Writing – review & editing, Methodology, Investigation. **Martina D'Alessandro:** Writing – review & editing, Visualization, Methodology, Investigation. **Brunella Grigolo:** Writing – review & editing, Supervision, Methodology, Investigation, Conceptualization. **Chiara Gualandi:** Writing – original draft, Visualization, Validation, Supervision, Methodology, Funding acquisition, Formal analysis, Data curation, Conceptualization. **Giovanna Desando:** Writing – original draft, Visualization, Validation, Supervision, Project administration, Methodology, Investigation, Funding acquisition, Formal analysis, Data curation, Conceptualization. **Maria Letizia Focarete:** Writing – review & editing, Validation, Supervision, Methodology, Data curation, Conceptualization.

Declaration of competing interest

The authors declare that they have no known competing financial interests or personal relationships that could have appeared to influence the work reported in this paper.

Acknowledgements

This work was supported by the Italian Ministry of Health, Progetto GR Ministero della Salute, Grant number: GR-2019-730639, A novel functionalized NUTraceuticals-laden hyaluronic hydrogel for gender-based PERsonalized treatment for osteoarthritis care: a novel proof-of-concept in viscosupplementation (NUTperOA), CUP: D39C21000030001.

Appendix A. Supplementary data

Supporting information (^{1}H NMR, amplitude sweep tests, viscosity flow curves, rotational sweep tests, time sweep tests, brightfield and fluorescence images at the inverted and epifluorescence microscope) are available free of charge. Supplementary data to this article can be found online at https://doi.org/10.1016/j.ijbiomac.2026.152190.

Data availability

Data will be made available on request.

References

[1] T.F. Moyad, Cartilage injuries in the adult knee: evaluation and management, Cartilage 2 (2011) 226–236, https://doi.org/10.1177/1947603510383973.
[2] G. Merkely, J. Ackermann, C. Lattermann, Articular cartilage defects: incidence, diagnosis, and natural history, Oper. Tech. Sports Med. 26 (2018) 156–161, https://doi.org/10.1053/J.OTSM.2018.06.008.
[3] A.J. Sophia Fox, A. Bedi, S.A. Rodeo, The basic science of articular cartilage: structure, composition, and function, Sports Health 1 (2009) 461, https://doi.org/10.1177/1941738109350438.
[4] M. Li, H. Yin, Z. Yan, H. Li, J. Wu, Y. Wang, F. Wei, G. Tian, C. Ning, H. Li, C. Gao, L. Fu, S. Jiang, M. Chen, X. Sui, S. Liu, Z. Chen, Q. Guo, The immune microenvironment in cartilage injury and repair, Acta Biomater. 140 (2022) 23–42, https://doi.org/10.1016/j.actbio.2021.12.006.
[5] R.F. Loeser, Osteoarthritis: a disease of the joint as an organ, Arthritis Rheum. 64 (2012) 1697–1707, https://doi.org/10.1002/art.34453.Osteoarthritis.
[6] J.S. Everhart, M.M. Abouljoud, D.C. Flanigan, Role of full-thickness cartilage defects in knee osteoarthritis (OA) incidence and progression: data from the OA initiative, J. Orthop. Res. 37 (2019) 77–83, https://doi.org/10.1002/jor.24140.
[7] S. Banerjee, K.S. Sahanand, Managing chondral lesions: a literature review and evidence-based clinical guidelines, Indian J. Orthop. 55 (2021) 252–262, https://doi.org/10.1007/S43465-021-00355-Z.
[8] M.C. Clegg TE, D. Caborn, Viscosupplementation with hyaluronic acid in the treatment for cartilage lesions: a review of current evidence and future directions, Eur. J. Orthop. Surg. Traumatol. 23 (2013) 119–124.
[9] N. Abraham, G. Pandey, T. Kolipaka, M. Negi, D.A. Srinivasarao, S. Srivastava, Exploring advancements in polysaccharide-based approaches: the cornerstone of next-generation cartilage regeneration therapeutics, Int. J. Biol. Macromol. 306 (2025), https://doi.org/10.1016/j.ijbiomac.2025.141352.
[10] F. Migliorini, A. Driessen, V. Quack, N. Sippel, B. Cooper, Y. El Mansy, M. Tingart, J. Eschweiler, Comparison between intra-articular infiltrations of placebo, steroids, hyaluronic and PRP for knee osteoarthritis: a Bayesian network meta-analysis, Arch. Orthop. Trauma Surg. 141 (2021) 1473–1490, https://doi.org/10.1007/S00402-020-03551-Y.
[11] L.W. Moreland, Intra-articular hyaluronan (hyaluronic acid) and hylans for the treatment of osteoarthritis: mechanisms of action, Arthritis Res. Ther. 5 (2003) 54, https://doi.org/10.1186/AR623.
[12] A. Migliore, G. Gigliucci, L. Alekseeva, R.R. Bannuru, T. Blicharski, D. Diracoglu, A. Georgiadis, H. Hamoud, N. Martusevich, M.M. Cerinic, J. Perduk, I. Szerb, T. Trč, X. Chevalier, Systematic literature review and expert opinion for the use of viscosupplementation with hyaluronic acid in different localizations of osteoarthritis, Orthop. Res. Rev. 13 (2021) 255–273, https://doi.org/10.2147/ORR.S336185.
[13] L.E. Miller, S. Bhattacharyya, W.R. Parrish, M. Fredericson, B. Bisson, R.D. Altman, Safety of intra-articular hyaluronic acid for knee osteoarthritis: systematic review and meta-analysis of randomized trials involving more than 8,000 patients, Cartilage 13 (2021) 351S–363S, https://doi.org/10.1177/1947603519888783.
[14] R.M. Irwin, E. Feeney, C. Secchieri, D. Galesso, I. Cohen, F. Oliviero, R. Ramonda, Distinct tribological endotypes of pathological human synovial fluid reveal characteristic biomarkers and variation in efficacy of viscosupplementation at reducing local strains in articular cartilage, Osteoarthr. Cartil. 28 (2021) 492–501, https://doi.org/10.1016/j.joca.2020.02.029.Distinct.
[15] J.M. Patel, K.S. Saleh, J.A. Burdick, R.L. Mauck, Bioactive factors for cartilage repair and regeneration: improving delivery, retention, and activity, Acta Biomater. 93 (2019) 222–238, https://doi.org/10.1016/j.actbio.2019.01.061.
[16] J. Faivre, A.I. Pigweh, J. Iehl, P. Maffert, P. Goekjian, F. Bourdon, Crosslinking hyaluronic acid soft-tissue fillers: current status and perspectives from an industrial point of view, Expert Rev. Med. Devices 18 (2021) 1175–1187, https://doi.org/10.1080/17434440.2021.2014320.
[17] U. Lindqvist, V. Tolmachev, K. Kairemo, et al., Elimination of stabilised hyaluronan from the knee joint in healthy men, Clin. Pharmacokinet. 41 (2002) 603, https://doi.org/10.2165/00003088-200241080-00004.
[18] D.J. Selig, A.T. Kress, I.M. Horton, J.R. Livezey, E.J. Sadik, J.P. DeLuca, Pharmacokinetics, safety and efficacy of intra-articular non-steroidal anti-inflammatory drug injections for the treatment of osteoarthritis: a narrative review, J. Clin. Pharm. Ther. 47 (2022) 1122–1133, https://doi.org/10.1111/jcpt.13669.
[19] A. Sulistio, F.M., et al., Intra-articular treatment of osteoarthritis with diclofenac-conjugated polymer reduces inflammation and pain, ACS Appl. Bio Mater. 2 (2019) 2822–2832.

[20] Z. Zhang, X. Wei, J. Gao, Y. Zhao, Y. Zhao, L. Guo, C. Chen, Z. Duan, P. Li, L. Wei, Intra-articular injection of cross-linked hyaluronic acid-dexamethasone hydrogel attenuates osteoarthritis: an experimental study in a rat model of osteoarthritis, Int. J. Mol. Sci. 17 (2016), https://doi.org/10.3390/ijms17040411.
[21] D.G. Miranda, L. de P. Ramos, N.F. dos S. Lopes, N.V.D.H.F. Silva, C.P. Soares, F. P. Rodrigues, V. de P. Morais, T. Sani-Taiariol, M.R. Baldan, L.M.R. de Vasconcellos, A.L.S. Borges, B. Grosgogeat, K. Gritsch, Ketoprofen associated with hyaluronic acid hydrogel for temporomandibular disorder treatment: an in vitro study, Gels 10 (2024), https://doi.org/10.3390/gels10120811.
[22] S. D'Adamo, S. Cetrullo, V. Panichi, E. Mariani, F. Flamigni, R.M. Borzì, Nutraceutical activity in osteoarthritis biology: a focus on the nutrigenomic role, Cells 2 (2020) 1–24, https://doi.org/10.3390/cells9051232.
[23] P. Makvandi, F. Della Sala, M. Gennaro, N. Solimando, M. Pagliuca, A. Borzacchiello, A hyaluronic acid-based formulation with simultaneous local drug delivery and antioxidant ability for active viscosupplementation, ACS Omega 7 (2022) 10039–11048, https://doi.org/10.1021/acsomega.1c05622.
[24] Y.S. Kim, F. Guilak, Engineering hyaluronic acid for the development of new treatment strategies for osteoarthritis, Int. J. Mol. Sci. (2022) 8662, https://doi.org/10.3390/ijms23158662.
[25] A. Zhao, E.H. Jeffery, M.J. Miller, Is bitterness only a taste? The expanding area of health benefits of Brassica vegetables and potential for bitter taste receptors to support health benefits, Nutrients 14 (2022), https://doi.org/10.3390/nu14071434.
[26] E.L. Connolly, M. Sim, N. Travica, W. Marx, G. Beasy, G.S. Lynch, C.P. Bondonno, J.R. Lewis, J.M. Hodgson, L.C. Blekkenhorst, Glucosinolates from cruciferous vegetables and their potential role in chronic disease: investigating the preclinical and clinical evidence, Front. Pharmacol. 12 (2021) 1–12, https://doi.org/10.3389/fphar.2021.767975.
[27] N. Mi ekus, K. Marszałek, M. Podlacha, A. Iqbal, C. Puchalski, A.H. Swiergiel, Health benefits of plant-derived sulfur compounds, glucosinolates, and organosulfur compounds, Molecules 25 (2020), https://doi.org/10.3390/molecules25173804.
[28] A. Aguilar-Galvez, D. García-Ríos, D. Ramírez-Guzmán, J. Lindo, R. Chirinos, R. Pedreschi, D. Campos, In vitro and in vivo biotransformation of glucosinolates from mashua (Tropaeolum tuberosum) by lactic acid bacteria, Food Chem. 404 (2023), https://doi.org/10.1016/j.foodchem.2022.134631.
[29] R.S. Combourieu B, L. Elfoul, A.M. Delort, Identification of new derivatives of sinigrin and glucotropaeolin produced by the human digestive microflora using 1H NMR spectroscopy analysis of in vitro incubations, Drug Metab. Dispos. 29 (2001) 1440–1445.
[30] R. Davidson, S. Gardner, O. Jupp, A. Bullough, S. Butters, L. Watts, S. Donell, M. Traka, S. Saha, R. Mithen, M. Peffers, P. Clegg, Y. Bao, A. Cassidy, I. Clark, Isothiocyanates are detected in human synovial fluid following broccoli consumption and can affect the tissues of the knee joint, Sci. Rep. 7 (2017), https://doi.org/10.1038/s41598-017-03629-5.
[31] H. Tang, K. Qin, A. Wang, S. Li, S. Fang, W. Gao, M. Lu, W. Huang, H. Zhang, Z. Yin, 3,3′-Diindolylmethane inhibits LPS-induced human chondrocytes apoptosis and extracellular matrix degradation by activating PI3K-Akt-mTOR-mediated autophagy, Front. Pharmacol. 13 (2022), https://doi.org/10.3389/fphar.2022.999851.
[32] D.L. Palliyaguru, J.M. Yuan, T.W. Kensler, J.W. Fahey, Isothiocyanates: translating the power of plants to people, Mol. Nutr. Food Res. 62 (2018), https://doi.org/10.1002/mnfr.201700965.
[33] E. Lucarini, L. Micheli, L. Di Cesare Mannelli, C. Ghelardini, Naturally occurring glucosinolates and isothiocyanates as a weapon against chronic pain: potentials and limits, Phytochem. Rev. 21 (2) (2022) 647–665, https://doi.org/10.1007/S11101-022-09809-0.
[34] D. Song, H. Liang, P. Kuang, P. Tang, G. Hu, Q. Yuan, Instability and structural change of 4-methylsulfinyl-3-butenyl isothiocyanate in the hydrolytic process, J. Agric. Food Chem. 61 (21) (2013) 5097–5102, https://doi.org/10.1021/jf400355d.
[35] F.S. Hanschen, E. Lamy, M. Schreiner, S. Rohn, Reactivity and Stability of Glucosinolates and Their Breakdown Products in Foods Angewandte, 2014, pp. 11430–11450, https://doi.org/10.1002/anie.201402639.
[36] C. Kühn, F. Kupke, S. Baldermann, R. Klopsch, E. Lamy, S. Hornemann, A.F. H. Pfeiffer, M. Schreiner, F.S. Hanschen, S. Rohn, Diverse excretion pathways of benzyl glucosinolate in humans after consumption of nasturtium (Tropaeolum majus L.)—a pilot study, Mol. Nutr. Food Res. 62 (2018) 1–12, https://doi.org/10.1002/mnfr.201800588.
[37] H. Choi, H. Kim, S. Han, H.W. Park, I.J. Ha, J.S. Kim, S.G. Lee, Antioxidant and anti-inflammatory activities of high-glucosinolate-synthesis lines of Brassica rapa, Antioxidants 12 (2023) 1–12, https://doi.org/10.3390/antiox12091693.
[38] A. López-vázquez, J.J. Garcia-bañuelos, A.S. González-garibay, S. Del Toro-arreola, M.R. Bueno-topete, S. Sánchez-enríquez, J.F. Muñoz-valle, L.F. Jave-suárez, J. Armendáriz-borunda, B.E. Bastidas, IRS-1 pY612 and Akt-1/PKB pT308 phosphorylation and anti-inflammatory effect of diindolylmethane in adipocytes cocultured with macrophages, Med. Chem. (Los Angeles) 13 (2017) 727–733, https://doi.org/10.2174/1573406413666170922095011.
[39] A.T. Dinkova-Kostova, R.V. Kostov, Glucosinolates and isothiocyanates in health and disease, Trends Mol. Med. 18 (2012) 337–347, https://doi.org/10.1016/j.molmed.2012.04.003.
[40] P.S. Sreeja, K. Arunachalam, D.T. de O. Martins, J.C. da S. Lima, S.O. Balogun, E. Pavan, S. Saikumar, S. Dhivya, M. Kasipandi, T. Parimelazhagan, *Sphenodesme involucrata* var. *paniculata* (C.B. Clarke) Munir.: chemical characterization, anti-nociceptive and anti-inflammatory activities of methanol extract of leaves, J. Ethnopharmacol. 225 (2018) 71–80, https://doi.org/10.1016/j.jep.2018.06.035.
[41] J.S. Shin, C.H. Yun, K.S. Chung, M.H. Bang, N.I. Baek, H.G. Chung, Y.W. Cho, K. T. Lee, Standardized ethyl acetate fraction from the roots of Brassica rapa attenuates the experimental arthritis by down regulating inflammatory responses and inhibiting NF-κB activation, Food Chem. Toxicol. 66 (2014) 96–106, https://doi.org/10.1016/j.fct.2014.01.025.
[42] L. Gambari, E. Pagnotta, L. Ugolini, L. Righetti, E. Amore, B. Grigolo, G. Filardo, F. Grassi, Insights into osteogenesis induced by crude Brassicaceae seeds extracts: a role for glucosinolates, Nutrients 16 (2024), https://doi.org/10.3390/nu16203457.
[43] H. Sadeghi, M. Mostafazadeh, H. Sadeghi, H. Sadeghi, V. Zarezade, A. Hadinia, E.P. Kokhdan, Further Evidence to Support Acute and Chronic Anti-Inflammatory Effects of *Nasturtium officinale*, n.d.
[44] R. Yazdanparast, S. Bahramikia, A. Ardestani, Nasturtium officinale reduces oxidative stress and enhances antioxidant capacity in hypercholesterolaemic rats, Chem. Biol. Interact. 172 (2008) 176–184, https://doi.org/10.1016/j.cbi.2008.01.006.
[45] D.P. Priya, S. Preetha, Effectiveness of Brassica juncea (mustard) plaster on reduction of knee pain and inability among geriatrics with osteoarthritis, J. Pharm. Bioallied Sci. 16 (2024) S2861–S2863, https://doi.org/10.4103/jpbs.jpbs_495_24.
[46] X. Zhao, S. Jiang, Q. Dong, J. Dang, Z. Liu, H. Han, Y. Tao, H. Yue, Anti-rheumatoid arthritis effects of iridoid glucosides from Lamiophlomis rotata (Benth.) kudo on adjuvant-induced arthritis in rats by OPG/RANKL/NF-κB signaling pathways, J. Ethnopharmacol. 266 (2021), https://doi.org/10.1016/j.jep.2020.113402.
[47] Y. Seong, G. Lin, B.J. Kim, H. Kim, S. Kim, S. Jeong, Hyaluronic acid-based hybrid hydrogel microspheres with enhanced structural stability and high injectability, ACS Omega (2019), https://doi.org/10.1021/acsomega.9b01475.
[48] X. Liu, D.P. Rodeheaver, J.C. White, A.M. Wright, L.M. Walker, F. Zhang, S. Shannon, A comparison of in vitro cytotoxicity assays in medical device regulatory studies, Regul. Toxicol. Pharmacol. 97 (2018) 24–32, https://doi.org/10.1016/j.yrtph.2018.06.003.
[49] J.G. Gomez-gutierrez, N. Bhutiani, M.W. Mcnally, P. Chuong, M.A. Jones, M. R. Zeiderman, W.E. Grizzle, L.R. Mcnally, The neutral red assay can be used to evaluate cell viability during autophagy or in an acidic microenvironment in vitro, Biothecnic Histochem. 96 (2022) 302–310, https://doi.org/10.1080/10520295.2020.1802065.The.
[50] S.P. Grogan, A. Barbero, V. Winkelmann, F. Rieser, J.S. Fitzsimmons, S. O'Driscoll, I. Martin, P. Mainil-Varlet, Visual histological grading system for the evaluation of in vitro-generated neocartilage, Tissue Eng. 12 (2006) 2141–2149, https://doi.org/10.1089/ten.2006.12.2141.
[51] C.H. Jeong, D.H. Kim, J.H. Yune, H.C. Kwon, D.M. Shin, H. Sohn, K.H. Lee, B. Choi, E.S. Kim, J.H. Kang, E.K. Kim, S.G. Han, In vitro toxicity assessment of crosslinking agents used in hyaluronic acid dermal filler, Toxicol. In Vitro 70 (2021), https://doi.org/10.1016/J.TIV.2020.105034.
[52] X. Xu, A.K. Jha, D.A. Harrington, M.C. Farach-Carson, X. Jia, Hyaluronic acid-based hydrogels: from a natural polysaccharide to complex networks, Soft Matter 8 (2012) 3280–3294, https://doi.org/10.1039/c2sm06463d.
[53] Y. Henrotin, R. Bannuru, M. Malaise, H.K. Ea, C. Confavreux, J. Bentin, D. Urbin-Choffray, T. Conrozier, J.P. Brasseur, P. Thomas, A.C. Hick, A. Marinello, N. Giordan, P. Richette, Hyaluronan derivative HYMOVIS® increases cartilage volume and type ii collagen turnover in osteoarhritic knee: data from MOKHA study, BMC Musculoskelet. Disord. 20 (2019) 1–16, https://doi.org/10.1186/S12891-019-2667-0/TABLES/9.
[54] E. Frisch, L. Clavier, A. Belhamdi, N.E. Vrana, P. Lavalle, B. Frisch, B. Heurtault, V. Gribova, Preclinical in vitro evaluation of implantable materials: conventional approaches, new models and future directions, Front. Bioeng. Biotechnol. 11 (2023), https://doi.org/10.3389/fbioe.2023.1193204.
[55] W. Li, J. Zhou, Y. Xu, Study of the *in vitro* cytotoxicity testing of medical devices, Biomed. Rep. 3 (2015) 617–620, https://doi.org/10.3892/br.2015.481.
[56] M.A. Nicholls, A. Fierlinger, F. Niazi, M. Bhandari, The disease-modifying effects of hyaluronan in the osteoarthritic disease state, Clin. Med. Insights Arthritis Musculoskelet. Disord. 10 (2017), https://doi.org/10.1177/1179544117723611.
[57] B.A. Buhren, H. Schrumpf, E. Bölke, K. Kammers, P.A. Gerber, Standardized in vitro analysis of the degradability of hyaluronic acid fillers by hyaluronidase, Eur. J. Med. Res. 23 (2018), https://doi.org/10.1186/S40001-018-0334-9.
[58] S. Azadi, H. Ashrafi, A. Azadi, Mathematical modeling of drug release from swellable polymeric nanoparticles article info abstract, J. Appl. Pharm. Sci. 7 (2017) 125–133, https://doi.org/10.7324/JAPS.2017.70418.
[59] L. Pourtalebi Jahromi, M. Ghazali, H. Ashrafi, A. Azadi, A comparison of models for the analysis of the kinetics of drug release from PLGA-based nanoparticles, Heliyon 6 (2020), https://doi.org/10.1016/J.HELIYON.2020.E03451/ATTACHMENT/E99A3BA2-59F5-40D3-880C-B93B0ABB4012/MMC1.DOCX.
[60] L.A. Solchaga, K.J. Penick, J.F. Welter, Chondrogenic differentiation of bone marrow-derived mesenchymal stem cells: tips and tricks, in: Methods in Molecular Biology, Humana Press Inc., 2011, pp. 253–278, https://doi.org/10.1007/978-1-60761-999-4_20.
[61] A.R. Armiento, M. Alini, M.J. Stoddart, Articular fibrocartilage - why does hyaline cartilage fail to repair? Adv. Drug Deliv. Rev. 146 (2019) 289–305, https://doi.org/10.1016/j.addr.2018.12.015.
[62] T. Hamada, T. Sakai, H. Hiraiwa, M. Nakashima, Y. Ono, H. Mitsuyama, N. Ishiguro, Surface markers and gene expression to characterize the differentiation of monolayer expanded human articular chondrocytes, Nagoya J. Med. Sci. 75 (1–2) (2013 Feb) 101–111 (PMID: 23544273; PMCID: PMC4345713).
[63] J. Wang, J. Ma, J.H. Gu, F.Y. Wang, X.S. Shang, H.R. Tao, X. Wang, Regulation of type II collagen, matrix metalloproteinase-13 and cell proliferation by interleukin-

1β is mediated by curcumin via inhibition of NF-κB signaling in rat chondrocytes, Mol. Med. Rep. 16 (2017) 1837–1845, https://doi.org/10.3892/mmr.2017.6771.
[64] P. Tikakosol, P.D. Topham, M.J. Derry, R. Somsunan, P. Worajittiphon, C. Manaspon, W. Punyodom, Kartogenin-encapsulated self-healing injectable hydrogel based on hyaluronic acid and chitosan derivative for use as viscosupplementation in knee osteoarthritis, Int. J. Biol. Macromol. 328 (2025), https://doi.org/10.1016/j.ijbiomac.2025.147304.
[65] J. Zhou, J. Liang, K. Yang, G. Zhang, Injectable hydrogels loaded with EGCG /KGN for the treatment of osteoarthritis, J. Biomater. Appl. 40 (2026) 819–829, https://doi.org/10.1177/08853282251379151.
[66] P. Chen, S. Zhu, Y. Wang, Q. Mu, Y. Wu, Q. Xia, X. Zhang, H. Sun, J. Tao, H. Hu, P. Lu, H. Ouyang, The amelioration of cartilage degeneration by ADAMTS-5 inhibitor delivered in a hyaluronic acid hydrogel, Biomaterials 35 (2014) 2827–2836, https://doi.org/10.1016/j.biomaterials.2013.12.076.
[67] R. Rieger, S. Kaderli, C. Boulocher, In vivo impact on rabbit subchondral bone of viscosupplementation with a hyaluronic acid antioxidant conjugate, BMC Musculoskelet. Disord. 25 (2024), https://doi.org/10.1186/s12891-024-07921-0.
[68] N.A. Householder, A. Raghuram, K. Agyare, S. Thipaphay, M. Zumwalt, A review of recent innovations in cartilage regeneration strategies for the treatment of primary osteoarthritis of the knee: intra-articular injections, Orthop. J. Sports Med. 11 (2023), https://doi.org/10.1177/23259671231155950.
[69] K. Zhou, X. He, Y. Liu, Z. Bei, K. Shi, D. Hu, Y. Wang, M. Gao, B. Chu, Q. Yang, C. Yang, Z. Qian, Advances in injectable hydrogel-based intra-articular treatment systems for osteoarthritis therapy, Chin. Chem. Lett. (2025) 111723, https://doi.org/10.1016/j.cclet.2025.111723.
[70] K.S. Kim, S.J. Park, J.A. Yang, J.H. Jeon, S.H. Bhang, B.S. Kim, S.K. Hahn, Injectable hyaluronic acid-tyramine hydrogels for the treatment of rheumatoid arthritis, Acta Biomater. 7 (2011) 666–674, https://doi.org/10.1016/j.actbio.2010.09.030.
[71] Y. Liu, J. Yang, Z. Luo, Development of an injectable thiolated icariin functionalized collagen/hyaluronic hydrogel to promote cartilage formation *in vitro* and *in vivo*, J. Mater. Chem. B (17) (2019), https://doi.org/10.1039/C9TB00211A.